8-1-2003

Modelling the tone reproduction characteristics of digital printers using continuous tone model

Prashant Mehta

Modelling The Tone Reproduction Characteristics of Digital Printers Using Continuous Tone Model

By

Prashant P. Mehta

B.E. (Chemical) L. D. College of Engineering, Ahmedabad, India

(1997)

A thesis submitted in partial fulfillment of the
requirements for the degree of Master of Science
in the Chester F. Carlson Center for Imaging Science
of the College of Science
Rochester Institute of Technology

August 2003

Signature of the Author_____

Accepted by_____ 11/11/2003

Coordinator, M.S. Degree Program Date

CHESTER F. CARLSON
CENTER FOR IMAGING SCIENCE
COLLEGE OF SCIENCE
ROCHESTER INSTITUTE OF TECHNOLOGY
ROCHESTER, NEW YORK

CERTIFICATE OF APPROVAL

M.S. DEGREE THESIS

The M.S. Degree Thesis of Prashant P. Mehta
has been examined and approved by the
thesis committee as satisfactory for the
thesis requirement for the
Master of Science degree

Dr. Jonathan S. Arney, Thesis Advisor

Dr. Peter Anderson

Dr. Jeffery Pelz

11/10/2003
Date

THESIS RELEASE PERMISSION

ROCHESTER INSTITUTE OF TECHNOLOGY
COLLEGE OF SCIENCE
CHESTER F. CARLSON
CENTER FOR IMAGING SCIENCE

Title of Thesis: Modelling The Tone Reproduction Characteristics of Digital Printers Using Continuous Tone Model

I, Prashant P. Mehta, hereby grant permission to the Wallace Memorial Library of R.I.T. to reproduce my thesis in whole or in part. Any reproduction will not be for commercial use or profit.

Modelling The Tone Reproduction Characteristics of Digital Printers Using Continuous Tone Model

by

Prashant P. Mehta

Submitted to the Chester F. Carlson Center for Imaging Science College of Science in partial fulfillment of the requirements for the Master of Science Degree at the Rochester Institute of Technology

ABSTRACT

Traditional halftone models have been used to characterize the tone reproduction characteristics of digital printers. These models can be corrected to incorporate system parameters like light scattering, softer dot edge etc. This thesis work explores the possibility of applying the modified continuous tone model to characterize the tone reproduction of high addressibility printers. Both the continuous tone model and the modified halftone model will be compared for how well they characterize the tone reproduction characteristics of the printer.

ACKNOWLEDGEMENTS

I wish to acknowledge wonderful and patient support of my thesis advisor Dr. Jonathan Arney. In the years that I have spent in Dr. Arney's guidance, I have come to respect his "healthy skepticism" approach to research.

Dr. Peter Anderson has been helpful in providing different prints that are used in this thesis for analysis. I am also thankful to Dr. Pelz for all his help on this project.

Had it not been for patience and persistence of my wife Vasanthi and my parents Pradeep and Mallika, I may have not been able to bring this project to a completion.

I also wish to thank my friends Kate Johnson and Joan Ashley for their support.

This research has been funded by Hewlett-Packard and I wish to extend my thanks for their financial support. And, the work was conducted in collaboration with Laboratory for Applied Computing.

- Contents -

- List of figures -

Chapter 1

Chapter 2

Chapter 3:

Chapter 4

Chapter 5

No figures

Appendix

- List of tables -

Chapter 1

Introduction

The purpose of this project was to develop and test a new model for tone reproduction in a 600 dpi electrophotographic laser printer. The project involved printing technology, digital halftoning, microdensitometry analysis, and halftone optical theory. Key background literature will be reviewed in this report, followed by a description of the results of the project.

Printing is a means of graphic communication that employs the reproduction of visual images, most often on paper. Printing and publishing are major businesses throughout the world. In the U.S. alone these businesses represent about 3 percent of the gross domestic product (GDP). There are more printing companies in the U.S. (60,000) than any other type of manufacturing company (Pocketpal, 1997). Although printing technology has been practiced commercially for many centuries, recent developments in digital technologies have stimulated recent advances in new printing technologies. Desktop printers based on ink jet and

electrophotography, for example, are the result of R&D efforts made over the past two decades.

Most printing technologies are intrinsically binary processes that either deliver or do not deliver ink to a given point on the paper. While this is very useful for reproducing letters, it is difficult to reproduce pictorial images with gray tones. To simulate pictorial gray tones, various techniques of spatial modulation are used. The most familiar halftone technique (AM screening) currently used is illustrated in Figure (1.1). Spatial modulation simulates a gray tone in a local region of an image by controlling the fraction of the local area that is printed (ink) and the fraction that is not printed (paper). This binary image, containing only black and white, is simple in concept, but it is complex in the way it behaves optically as will be described in sections 2.2 and 2.3.

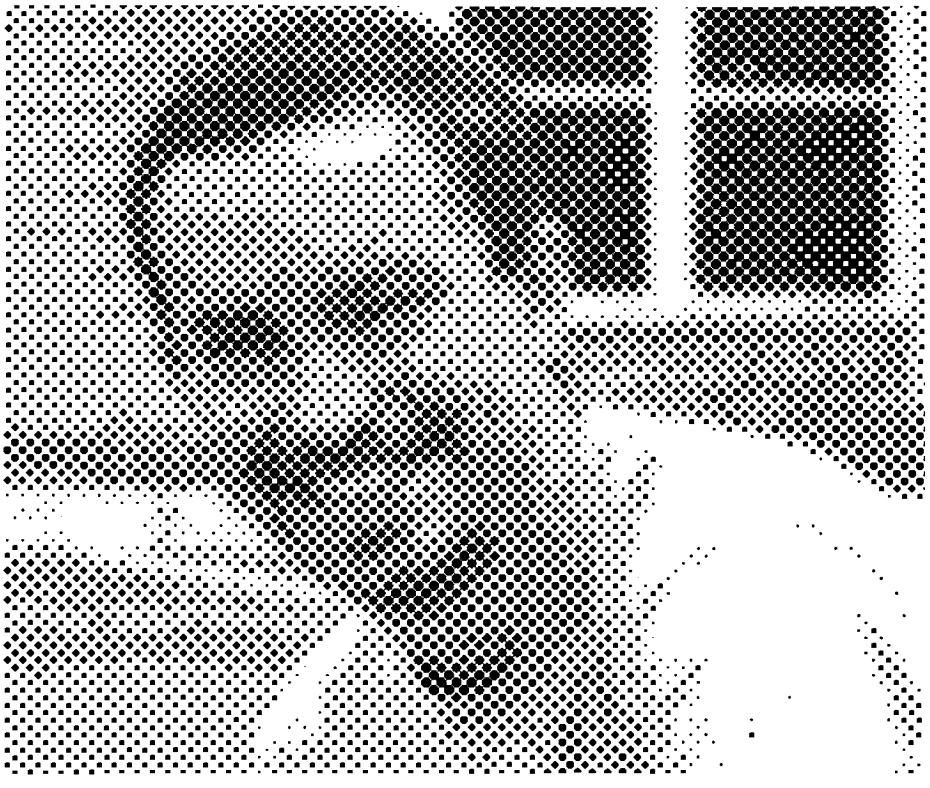

Figure 1.1: Halftone Image
(Note: The size of the dots is exaggerated in the above image to better illustrate the halftoning technique)

The printing technology of concern in this report is laser electrophotography (EP), and the halftone techniques that will be addressed are typically used to produce pictorial images with electrophotographic printers. Section 2.3.3 will review recent literature reports on the optical behavior of digital halftones. However, the behavior of printed halftone samples from a high-resolution (600 dpi) EP printer suggested that it may be useful to model the optical behavior of the process with a continuous tone

model rather than a halftone model. Whether a continuous tone or halftone model was applied, it was found that modifications were required to fit experimental data. The halftone model required modifications to account for effects characteristic of continuous tone systems, and the continuous tone model required modifications to account for spatial effects characteristic of halftone systems. Whether the printed image behaved more like a halftone or a continuous tone depended on the overall spatial frequency characteristics of the system. Thus it is important to understand the spatial characteristics of both the printing systems and the halftone algorithms.

The spatial characteristic of an electrophotographic printer is determined by its addressability. The addressability of the printer is defined as the number of dots per inch that a given printer is designed to place on the page, typically expressed in dots per inch (dpi), such as a "300 dpi printer". To understand the influence of addressability on the new modified continuous tone model, experiments were conducted with printers of two different addressabilities: a Hewlett-Packard Color LaserJet 4000 (addressability: 300 dpi) and Hewlett-Packard Color LaserJet 4500 (addressability: 600 dpi). To understand the influence of the spatial

characteristics of the halftoning algorithms on the new model, different types of digital halftones were examined as well. These included a Floyd-Steinberg algorithm, a clustered dot algorithm and a linear pixel shuffling algorithm, as described in Section 2.2. All samples examined in this project were printed on plain, non-coated paper using either black or cyan toner.

Chapter 2 of this report contains the background literature review. It explains the mechanism of laser EP printers (section 2.1). The halftoning algorithms used in this study are described in section 2.2, and published literature on halftone models is reviewed in section 2.3.

Chapter 3 discusses the behavior of printed halftone samples from EP printers. Section 3.1 and 3.2 contain observational comments. A halftone model based on probability theory (Arney-Tsujita, 1999, Arney-Yamaguchi, 1999 and Arney-Alber, 1998) was applied to the experimental samples in this project. This is described in section 3.3.

Chapter 4 contains most of the experimental work done for this dissertation. It begins with a description of a simple continuous tone model based on Beer-Lambert theory (section 4.1 and 4.2). The remaining sections of Chapter 4 discuss how the

printed samples differ from this simple continuous tone model and how to modify the model to account for observed behavior. The last section in Chapter 4 compares the relative utility of the continuous tone and halftone models.

Chapter 5 contains conclusions of this study and discusses directions for further experimental work. Appendix A contains details of experimental procedures employed in this paper.

Chapter 2

Background Literature Review

This chapter provides a brief review of the key technologies involved in the project. The basic printing mechanism of electrophotographic printers is described in section 2.1. Section 2.2 discusses the halftoning process in details. The models for characterizing the tone behavior of the printed halftones are discussed in sections 2.3 and 2.4.

2.1 Electrophotographic Printers

The project was carried out using two laser printers based on the electrophotographic process. In order to understand the tone reproduction behavior of these systems, it is helpful to be familiar with the basic mechanism of this printing process. Electrophotography, sometimes referred to as xerography, is the reproduction process used in laser printers and office copy machines (Pocketpal, 1997; Wilson, 1997; Sturge-Walworth-Shepp, 1989). The input for a copy machine is a hard copy document, but for a laser printer the input is a signal from a computer. In conventional

copiers, the light from a source illuminates the surface of the document to be copied and the document is imaged on the surface of a photoconductor. In a laser printer, light from a modulated and raster-scanned laser forms the image by exposing a photoconductive material, as illustrated in Figure 2.1.

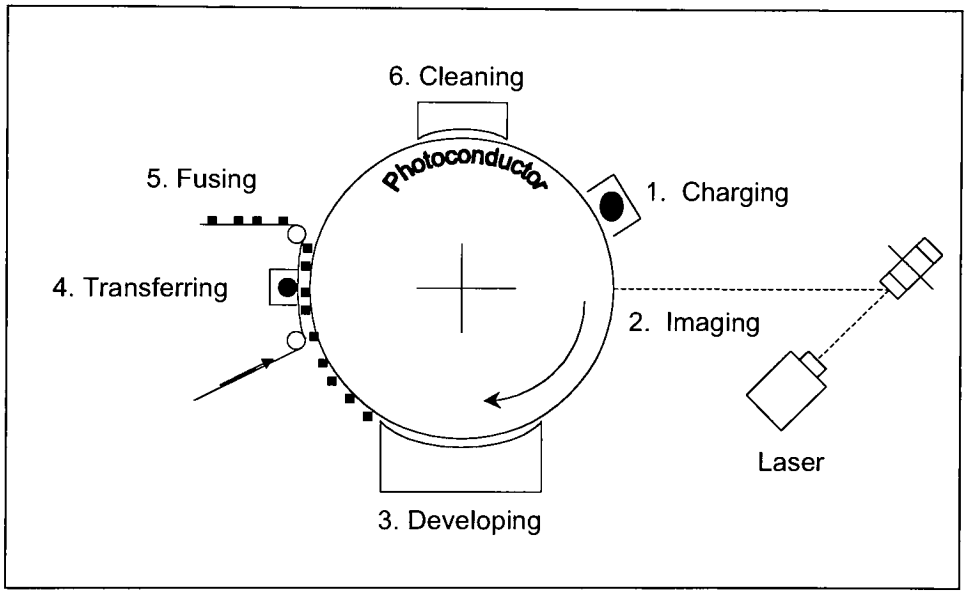

Figure 2.1: *Mechanism of electrophotographic printers*

The electrophotographic process uses a photoconductor in the form of either a rigid drum, as illustrated in Figure 2.1, or a flexible belt made from organic material. The surface consists of a thin photoconductive material with an ohmic resistance that changes when exposed to light. The surface is electrically charged (step 1 in

Figure 2.1), and an imagewise exposure results in an imagewise dissipation of charge (step 2 in Figure 2.1). The latent image, composed of a spatial distribution of charge, is then developed as shown in Figure 2.1, step 3, where toner particles are charged in a way to transfer to either the exposed or the not-exposed part of latent image. In most laser printers the exposed region is the region that is toned. The toner is then transferred to paper and fused to the surface under heat and/or pressure as illustrated in Figure 2.1, steps 4 and 5.

2.2 Halftoning

All of the images printed for this project were produced with digital halftone algorithms. The electrophotographic process is capable of some degree of continuous tone control (by controlling the intensity of the laser and ultimately the charge caused on the photoconductive drum), but high quality pictorial images from these printers require halftoning. The following is a brief review of the basic concepts of halftoning and digital halftoning.

2.2.1 The Origins of the Halftone Process

Except for a few printing techniques (gravure and collotype), it is not possible to reproduce more than two levels of tone in printing processes; black and white (Sturge-Walworth-Shepp, 1989). Thus, tone is typically simulated by some method of spatially distributing the ink (or colorant) on the paper, as illustrated in Figure 2.2. Spatial modulation techniques for simulating tone in printed images have been practiced for at least 500 years.

Figure 2.2: Copperplate engraving of Johann Gutenberg by André Thevet, Paris, 1584, from the RIT Cary Collection. Detail on the right illustrates spatial modulation.

In the halftone technique, the illusion of tone in a given region of an image is created by varying the fraction of the region that is covered by ink. The basic theory of the halftone is described by the Murray-Davies equation (2.1) in which the overall image reflectance, R, is determined by the reflectance of the ink, R_i; the fraction of the image that is covered by the ink, F; the reflectance of the paper, R_p; and the fraction of the image that is paper, 1 F. (refer Engeldrum, 1996 for a more comprehensive review of halftone theory)

$$R = F \cdot R_i + (1-F) \cdot R_p \tag{2.1}$$

The objective of any halftone process is to make the halftone dots small enough so the eye at a normal reading distance cannot resolve them. Varying the dot area fraction, F, in the printing process controls the visual tone level, R.

2.2.2 Halftones for Digital Printers

Most desktop digital printers are binary in nature and use halftone techniques to simulate tone. The spatial addressability of these printers is less by an order of magnitude than that of high

volume printing systems. Therefore, the traditional halftone algorithms developed for high volume printing are inadequate for digital printers. Significant research has been reported over the past two decades on the development of halftone algorithms especially suited for digital printing. These algorithms generate a binary halftone image by comparing the pixels of original continuous-tone image to a threshold value. Digital halftoning has become a significant subset of the digital image processing discipline today.

Digital halftoning techniques are classified in two main categories: amplitude modulation (AM in short) screening and frequency modulation (FM) screening. The AM screening technique, used extensively for the past 130 years, controls F by varying the size of the halftone dots while maintaining a constant distance between the dot centers. In the last two decades, significant numbers of algorithms have been developed that control dot area fraction, F, by the number of dots printed per unit area in the image. The size of a dot is kept constant in this process. This is the frequency modulation or FM screening (Wilson, 1997).

Whether AM or FM, a digital halftone is designed based on a matrix representing the addressability of the printer, as illustrated in Figure 2.3. The example shown in the figure 2.3 is of 300dpi

printer, and therefore each individual element of the matrix, called printer spot, is of the size 1/300" × 1/300". Each element in this matrix represents a location where a dot of ink could be placed or not placed. Different types of digital halftone algorithms have been developed to control the placement of ink (or colorant) dots.

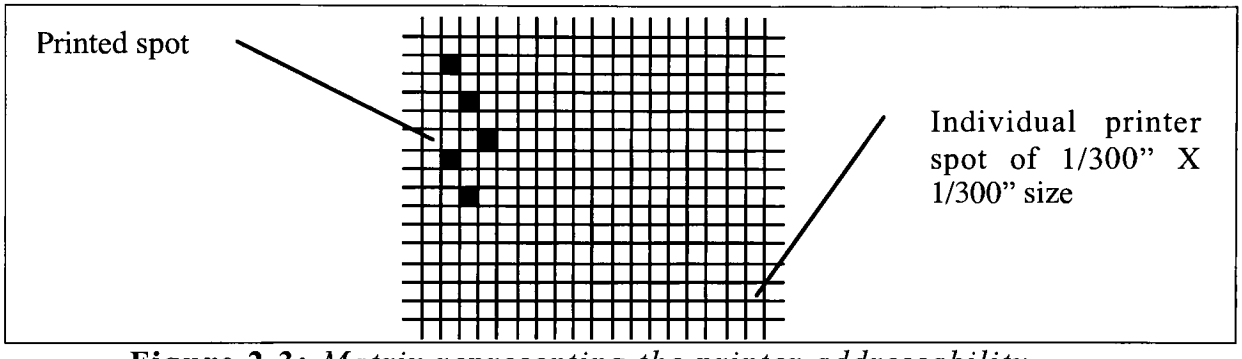

Figure 2.3: *Matrix representing the printer addressability*

According to the screening technique used the digital halftone can be divided into two classes: (a) clustered and (b) dispersed.

2.2.3 Clustered Dot

This is the most frequently used technique in the publishing and graphic arts industries. Digital halftones are produced by breaking the output image down into halftone cells, where each cell can contain a single halftone dot. Each halftone dot is made up of

several printer pixels (individual addressable cells shown in the Figure 2.3). These pixels are either turned on (making them black) or turned off (leaving them white) by the printer (laser beam or ink-jet printhead).

In a binary printer, the number of tones that can be reproduced is limited by the size of the cell. A cell containing n × n printer elements will produce $n^2 + 1$ gray levels. For example, a 2x2 cell can reproduce 5 gray tones.

For a given tone to be reproduced, it must be decided whether each pixel in the cell should be black or white. For that purpose, a threshold matrix is used whose elements correspond to each pixel of the cell. These thresholds determine the gray tone at which the printer pixel is turned on. For example, for a reflectance gray value of 10 percent ($0 < I < 100$), all elements with a threshold value, T, less than or equal to 10 will be turned on. Thus, the entire output plane is covered with regular patterns of threshold values. That is to say, each pixel of the printer is assigned a threshold value.

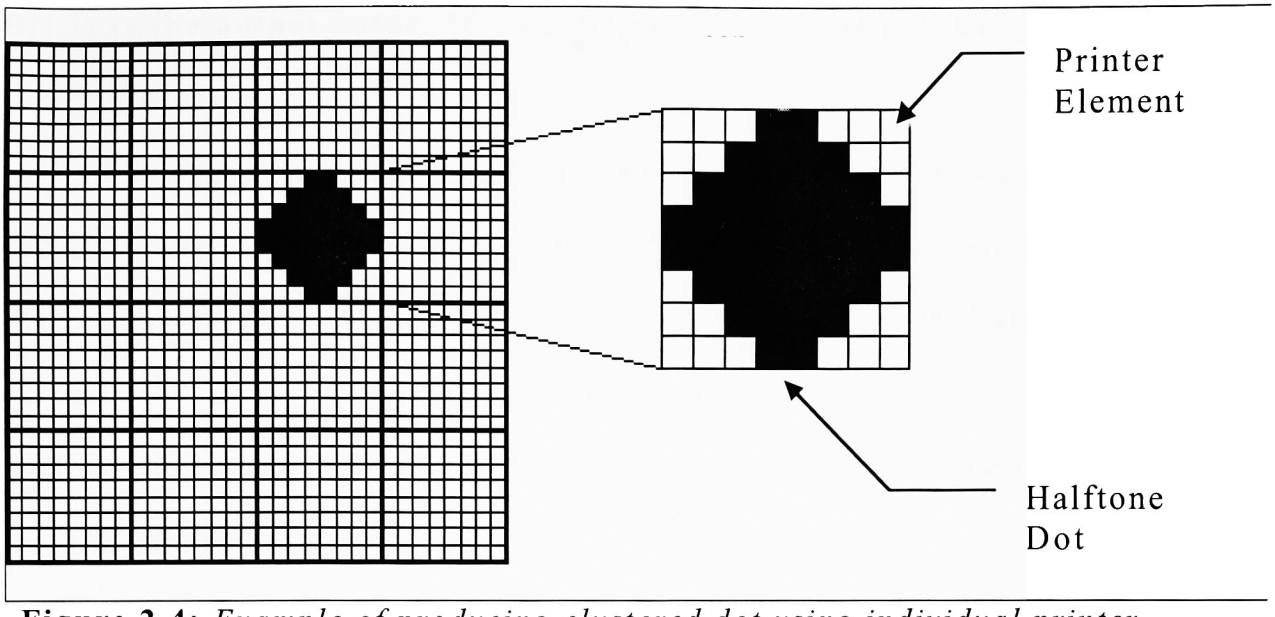

Figure 2.4: *Example of producing clustered dot using individual printer spots*

The reproduction process is to assess each pixel of the output plane, and compare the threshold value to the gray value of the input image to determine which pixels are turned on. The condition used is given by:

$$B(i,j) = \begin{cases} 0, \text{ if } I(i,j) \leq T(i,j) \\ 1, \text{ if } I(i,j) > T(i,j) \end{cases}$$

B(i,j) is the output value, I(i,j) the input gray level and T(i,j) the threshold value

The reason that this method is called clustered dot is due to the structure of the threshold matrix. Thresholds are ordered such that each subsequent tone would result in adjacent pixels being turned "on" at discrete locations in printable area. This results in a pattern of dots that change in size as the tone level increases.

2.2.4 Dispersed Dot

The only characteristic of dispersed dot that is different from the clustered dot is the threshold matrix. In the previous method, the matrix elements with close values were grouped in the matrix. In the dispersed method, the threshold values are uniformly distributed in the matrix. The generation of the output image is the same as in the clustered dot method. Tone values are compared with threshold values and pixels are turned on or left off accordingly. The commonly used threshold matrix for dispersed dot is defined by Bayer (Bayer, 1973). Figure 2.5 shows a gray ramp created with both clustered dots and dispersed dots using Bayer's method

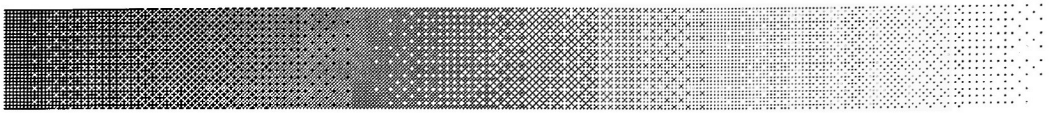

(a)

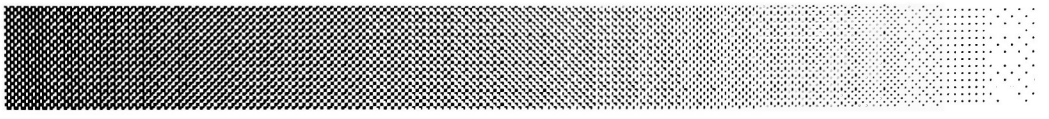

(b)

Figure 2.5: Gray wedge printed with (a) Clustered dot (b) Dispersed dot

2.2.5 Noise Power in Halftone Images:

The halftoning process creates an illusion of continuity of tone only if the halftone dots are smaller than the eye can see. A 5x5 clustered halftone dot printed with either a 300 or 600 dpi printer will result in visually detectable dots. The magnitude of spatial variations in halftone systems is often represented as the Root Mean Squared (RMS) deviation in the reflectance of the image. This is called the noise of the image, σ, and σ^2 is called the power of that image. The magnitude of the noise power varies with spatial frequency. The frequency spectrum of noise power is called the noise power spectrum, or sometimes the Wiener spectrum (Arney-Yamaguchi, 1999 and Dainty-Shaw, 1974) .

The human visual system attenuates the noise power of a halftone at higher frequencies. This is another way of saying that if the halftone dots are small enough, they will be too small to be seen by the human eye. If significant low frequency power is present in the halftone image, it will generally be visually detectable and potentially disturbing. The halftoning algorithms that create patterns with less power at lower frequencies and move the power to higher frequencies generally produce better looking images. The process of moving power to higher frequencies is called blue noise shifting. More information on this can be found in reference: Ulichney, 1987. Well defined masks for dispersed dot halftoning can shift halftone noise to higher frequencies. Another algorithm for digital halftoning called error diffusion also can shift noise to higher frequency.

2.2.6 Floyd Steinberg halftone:

The main idea behind the error diffusion technique is to compute the best approximation for each output pixel (whether to print it or not to print it), to determine the error between the actual value and the output value and spread it to the neighboring pixels. The error diffusion algorithm was first introduced by Floyd and

Steinberg in 1975 (Floyd-Steinberg, 1975, Floyd-Steinberg, 1976) and is often referred to as the Floyd-Steinberg algorithm. This algorithm transforms a gray scale image, I, with reflection gray values in the interval [0 < I <1], to a black-and-white image, B, with values of either 0 or 1. The psuedocode describing the error diffusion algorithm is shown below:

```
for every pixel position i,j in I
if I[i][j] < 0.5
  then B[i][j] = 0 (print a dot of ink)
  else B[i][j] = 1 (do not print a dot of ink)
error = I[i][j]   B[i][j]
distribute the error among unprocessed neighbors of i,j
```

The order of pixel visitation generally takes the form of raster processing:

```
for ( i = 0; i < i_max; i++ ) {
  for ( j = 0; j < j_max; j++ ) {
    process pixel i,j
  }
}
```

The input and output image dimensions are i_max by j_max. Floyd and Steinberg's error diffusion algorithm follows this pixel

ordering and distributes the error to four unprocessed neighbors of I[i][j] according to the following kernel:

$$\frac{1}{16}\begin{bmatrix} & P & 7 \\ 3 & 5 & 1 \end{bmatrix}$$

where P denotes the pixel currently being processed.

The neighbors can be written as:

I[i][j+1] = I[i][j+1] + error * 7/16

I[i+1][j-1] = I[i+1][j-1] + error * 3/16

I[i+1][j] = I[i+1][j] + error * 5/16

I[i+1][j+1] = I[i+1][j+1] + error * 1/16

Although an image produced through this algorithm has only two levels, the visual appearance captures the full grayscale range and detail of the original image. However, the image processed using the Floyd-Steinberg algorithm is often found to contain worm-like artifacts in very dark and very light regions.

A few samples of halftone images created through Floyd-Steinberg halftoning technique are shown in figure 2.6.

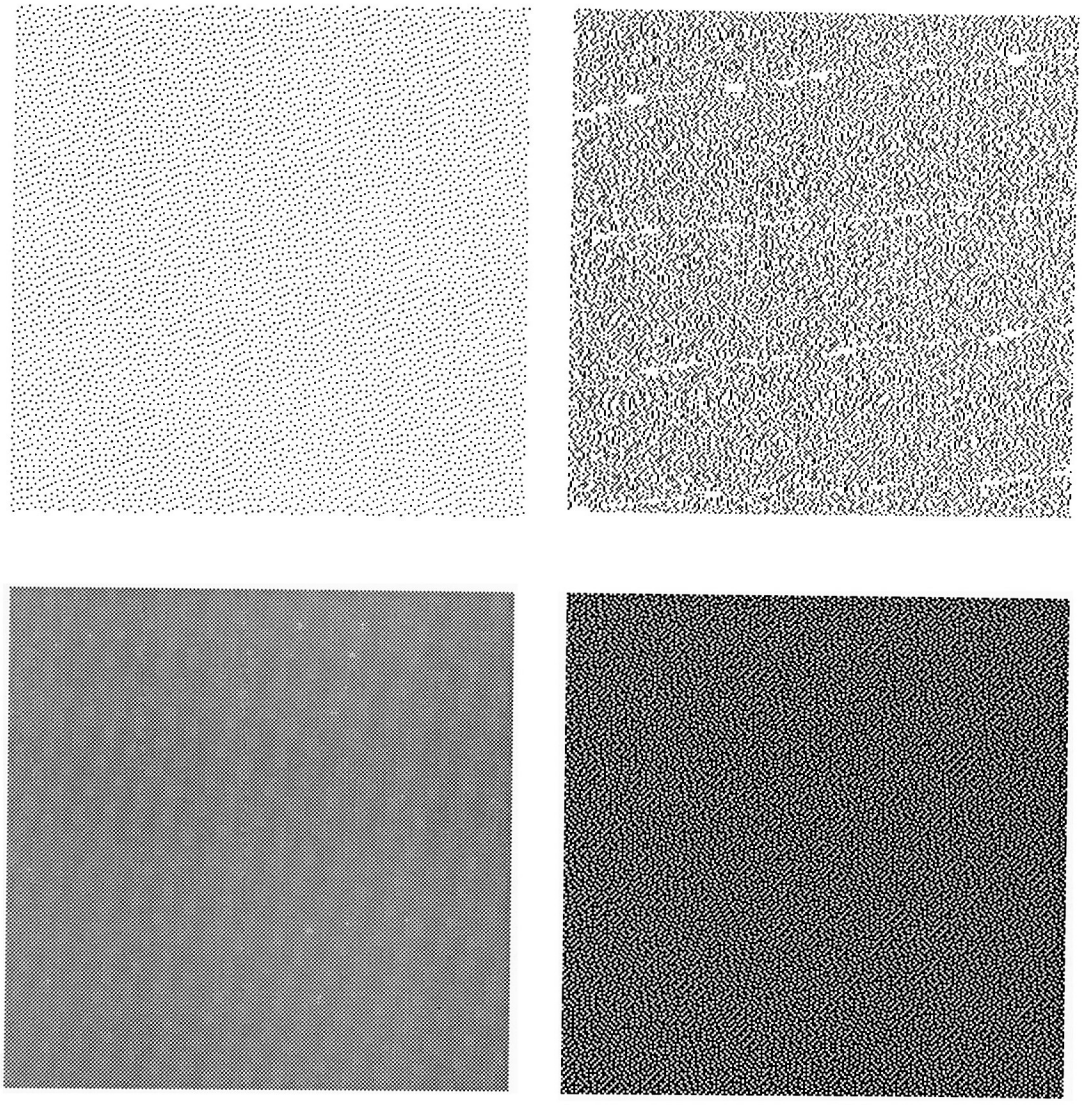

Figure 2.6: Examples of Floyd-Steinberg Halftones(The size of dots enlarged for demonstration purpose)

2.3 Literature review of tone reproduction behavior of halftones

Many researchers and authors have contributed to a more thorough understanding of the optical properties of halftone images. This section reviews the literature on halftone models.

2.3.1 Murray-Davies equation

An ideal halftone image contains dots of reflectance R_i on paper of reflectance R_p. Based on the law of conservation of energy, one would expect the total reflectance of the image, R, to be the sum of the photon energy from the dots and from the paper between the dots. This is expressed in equation (2.1) where F and (1-F) are the area fractions of the dots and the paper, respectively. Equation (2.1), is often called the Murray-Davies equation (Murray, 1936).

$$R=F\cdot R_i + (1-F)\cdot R_p \qquad (2.1)$$

In assuming the amount of reflection is linearly dependent on the relative amounts of ink and paper over the surface, the Murray-

Davies equation inherently assumes that the halftone dots are spatially uniform, are well defined, the absorption probabilities R_i and R_p are constants independent of the value of F, and only direct reflection occurs in the surface (i.e. before reaching the observer light does not reflect more than once from ink or paper surface). In reality, this is far from true. If one writes equation (2.1) as shown in 2.2, where R_k is R_i at F = 1and R_g is R_p at F = 0 then the equation does a very poor job of modeling R versus F. This is illustrated in Figure 2.7.

$$R=F\cdot R_k + (1-F)\cdot R_g \qquad (2.2)$$

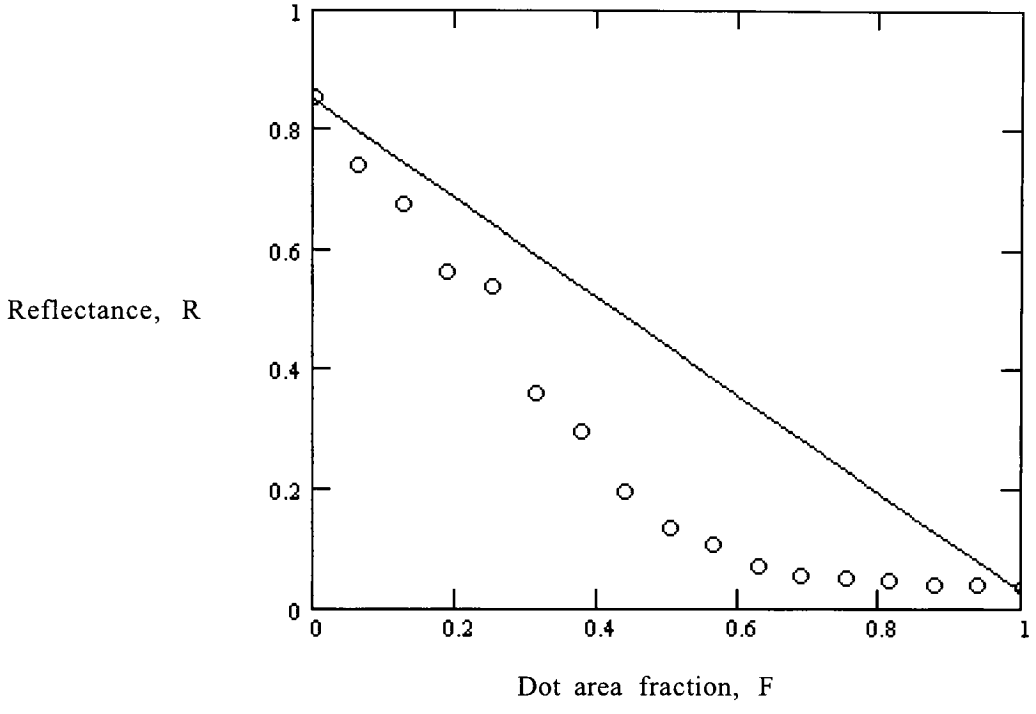

Figure 2.7: Reflectance vs Dot area fraction, individual points are the measured data and continuous line represents Murray Davis Equation

2.3.2 The Yule-Nielsen equation

It is generally observed that a printed image appears darker than one would expect based on the nominal size of the dot intended by the printing process. This phenomenon is referred to as physical dot gain and is the difference of the measured dot area fraction, F, and the nominal dot area fraction, F_n (signal sent to the printer). Physical dot gain can be caused by many factors. In the case of EP

printers, physical dot gain is caused in part by local dispersion of electric charge on the photo conductor drum, which causes unwanted toner particles to transfer onto the paper.

If one uses the actual dot area, F, rather than the value sent from the computer to the printer, F_n, equation (2.1) still generally results in a value of R that is lower than the measured value of R. This effect, which is different from physical dot gain, is called optical dot gain or the Yule Nielsen effect (Yule-Nielsen, 1951).

An empirical function often found to be a useful model for halftones is the Yule-Nielsen Equation (2.3).

$$R = \left[F \cdot R_k^{1/n} + (1-F) \cdot R_g^{1/n}\right]^n \tag{2.3}$$

Equation (2.3) is an empirical equation and has been found quite successful to describe the nonlinear relationship between R and F. Moreover, it is common practice to use the nominal dot fraction, F_n, from the printer instead of F in equation (2.2) and empirically correct for both physical and optical dot gain. The value of n can be determined experimentally to achieve the best fit between equation (2.2) and measured values of R and F or F_n. The study performed by Ruchdeschel and Hauser showed that $1 \leq n \leq 2$ (Rockdeschel-hauser, 1978).

Consider an element light source that strikes the dot

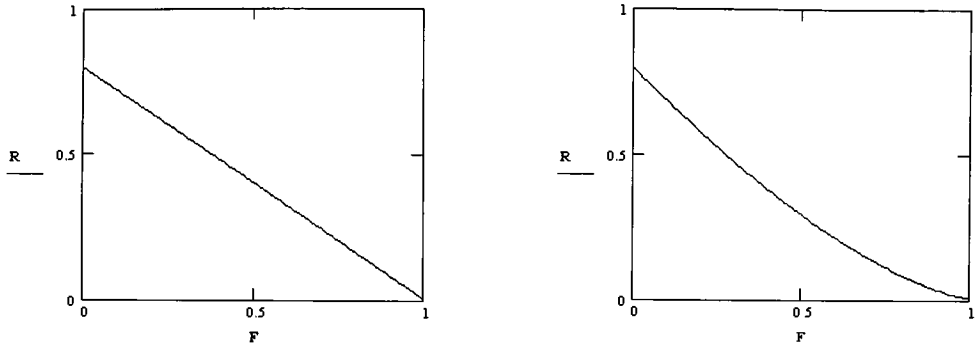

Figure 2.8: R vs. F modeled by Yule-Nielsen equation for n=1 and n=1.7.

Each different printing process has its own mechanistic causes for physical dot gain. However, optical dot gain has a single cause that is common to all methods of printing on paper. Optical dot gain is caused by the lateral scattering of light within the paper substrate. (Yule-Nielsen, 1951, Arney-Engeldrum-Zeng, 1995). Mechanistic studies have shown that if the scattering distance of the light in the paper is long relative to the size of the halftone dots, then the Yule-Nielsen equation is mechanistically correct with n = 2 (Engeldrum, 1994). For shorter scattering distances, the Yule-Nielsen equation is only an empirical approximation of optical dot gain, and numerous authors have published other models of R versus F based on mechanisms of light scattering in paper.

2.3.3 Recent developments in mechanistic halftone modeling

The Murray-Davies equation is essentially an expression of the law of conservation of energy. If a halftone image consists of two reflection populations, R_i and R_p, then the Murray-Davies equation (2.1) must be correct, and the non-linear relationship between R and F must be caused by a non-linear relationship for R_i vs F and/or R_p vs F. Experimentally, both R_i and R_p are observed to vary with F. Thus, a mechanistic model of R versus F can be developed if the functions for R_i vs F and R_p vs F can be modeled. Halftone models of this kind have been reported by Arney, et al. (Arney-Engledrum-Zeng, 1995, Arney-Yamaguchi, 1999, Arney-Tsujita, 1999).

The R_i vs F and R_p vs F models were initially derived empirically based on measured data on R_i vs F and R_p vs F. Instead of a single empirical n factor, the model contains two empirical parameters w and v. Parameter v relates to the distribution of colorant within the dot and w relates to the optical spread function of the paper. Estimates of these parameters are chosen empirically to fit image microstructure data on R_i vs F and R_p vs F (Arney-Eengledrum-Zeng, 1995, Arney-Yamaguchi, 1999, Arney-Tsujita, 1999). This model provides an excellent fit with the mean

reflectance, R versus F data as well as with R_i vs F and R_p vs F. This model was also applied in the analysis of the halftone data generated in the current thesis project. Results will be presented in subsequent sections.

Further work reported in the literature has explored the mechanistic relationship between the area fraction, F, and the reflectance values of R_i and R_p. This work involves mean level probability functions, P_{ij}. The values of P_{ij} represent the probability for the scattering of light from region *i* of area fraction f_i to region *j* of area fraction, f_j (Rogers, 1998, Arney-Wu-Blehm, 1998). For an ordinary black & white halftone for example, $F = f_1$ and $(1-F) = f_0$.

Previously, the P_{ij} functions were written empirically to fit observed data or determined by convolution calculations involving the paper point spread function, PSF, and the transmittance geometry of the halftone pattern, T(x,y). Recent work shows that P_{ij} can be deduced from symmetry properties of light scattering in paper and symmetry properties of the halftone pattern (Arney-Yamaguchi, 1999). A subsequent publication also shows how to account for higher ink opacity and softer dot edges (Arney-Tsujita, 1999).

2.3.4 The probability model used in this project

Tone reproduction characteristics of halftone images can be modeled with knowledge of the probability function, P_{00}, for light to reflect from the paper back out between the halftone dots after having entered the paper between the halftone dots (Arney-Yamaguchi, 1999). The other probability functions are related to P_{00} through equations (2.4) and (2.5). Note that $f_1 = F$ and $f_0 = (1-F)$, so the probability values, P_{ij}, are functions of F.

Arney and Yamaguchi also demonstrated that the reflectance functions, R_i and R_p vs F can be calculated from the probability functions as shown in equations (2.6) and (2.7), where T_0 and T_1 are the transmittance values of material above regions 0 and 1 respectively. In general, one assumes Beer-Lambert colorant layer of transmittance T_1. For a single ink system, $T_0=1$ is the transmittance of air.

$$P_{10} = 1 - P_{00} \tag{2.4}$$

$$P_{11} = 1-(1-P_{00})\cdot(f_0/f_1) \tag{2.5}$$

$$R_p = R_g\cdot T_0\cdot(P_{00}\cdot(T_0-T_1) + T_1) \tag{2.6}$$

$$R_i = R_g\cdot T_1\cdot(P_{11}\cdot(T_1-T_0) + T_0) \tag{2.6}$$

Thus, with knowledge of P_{00} versus F one can model R_i and R_p versus F and then R versus F.

2.3.5 Modelling P_{00} for Different Halftone Systems

Based on experimental and theoretical studies reported for a variety of different types of halftone systems, P_{00} versus F functions can be modeled as shown in equations (2.10) and (2.11) (Arney-Wu-Blehm, 1998).

$$P_{00} = 1 \quad w(1 \quad (1-F)^B) \tag{2.10}$$

$$P_{00} = 1 \quad F\cdot(2 \quad F^w \quad (1 \quad F)^w) \tag{2.11}$$

Equation (2.10) describes FM halftones such as those produced by the Floyd-Steinberg algorithm. Equation (2.11) describes clustered dot halftones. In both cases w is a parameter $0 \le w \le 1$ related to the degree of light scattering in the paper. (Arney-Arney-Katsube-Engledrum, 1996). The case $w=1$, corresponds to infinite light scattering distances in paper, and $w=0$ represents zero scattering. The term B is an empirical term adjusted to fit the data.

Modeling is done by first selecting the appropriate expression for P_{00} and using it to calculate equations (2.4), (2.5), (2.6), and (2.7). The results are then used with equation (2.1). The result is a model of R versus F for a halftone with Beer-Lambert ink with

uniform ink distribution in the printed dots. If the ink has a significant scattering coefficient or if the ink is not uniformly distributed across the halftone dot, then modifications can be made as described in the following section.

2.3.6 Ink Scattering and Dot Sharpness

The following techniques have been shown to be useful modifications to the halftone model (Arney-Tsujita, 1999).

First, the transmittance of the air is $T_0 = 1$ in equations (2.5) and (2.7). If the ink has a significant scattering coefficient, then the Beer-Lambert assumption does not apply. In such cases one can define the ink transmittance as $T_1 = T_{KM}$ where T_{KM} is the transmittance of an absorbing and scattering ink given by Kubelka-Munk theory, equation (2.8).

$$T_{KM} = \frac{b}{a \cdot \sinh(bSx) + b \cdot \cosh(bSx)} \tag{2.8}$$

In this equation, x= ink layer thickness at F=1

K = Kubelka-Munk absorption coefficient in mm^{-1}

S = Kubelka-Munk scattering coefficient in mm^{-1}

$a = (K/S+1)$ and $b = (a^2-1)^{0.5}$

In addition to scattering of light in the ink, the sharpness of the halftone dot can significantly perturb the model. In particular it

is often observed experimentally that dot edges are not sharp but show a progressive decline in ink amount, feathering into white between the dots. Such systems do not show clearly defined edges, and the concept of a distinct dot edge is more difficult to apply with confidence. In the current work the dot edge was defined as the region of most rapid spatial change in reflectance, dR/dx = maximum. This may not be the region where ink quantity reaches zero, but it is a region that can be identified and measured repeatably. Experimentally the dot edge is determined in image micrographs by a histogram analysis. The edge is identified as the value of R at lowest occurrence where dH/dR = minimum for histogram H(R). Segmentation at this value of R provides a repeatable measure of dot area fraction, F.

A consequence of defining the dot edge in this way is the need to modify the definitions of T_0 and T_1 in equations (2.6) and (2.7). We define T_0 and T_1 as shown in equations (2.9 and 2.10),

$$T_0 = 1-(1-T_{KM})\cdot(1-(1-F)^{\nu}) \tag{2.9}$$

$$T_1 = 1-(1-T_{KM})\cdot F^{\nu} \tag{2.10}$$

where T_{KM} is defined in equation (2.7). The value of ν is an empirical parameter adjusted to provide the best fit between the

model and experimental data. A value of $v = 0$ corresponds to perfectly sharp dot edges.

The procedure for fitting the model to experimental data was as follows. Starting values of w and v were selected. Then the model for P_{00} was chosen (equation (2.10) or (2.11)). Scattering and absorption coefficients S and K for the ink were assumed and applied to equation (2.7). Then equations (2.9) and (2.10) provided values of T0 and T1 which were used instead of T_0 and T_1 in equations (2.4), (2.5), (2.6), and (2.7). Finally, the values of R_i and R_p from (2.6) and (2.7) were used in equation (2.1) to calculate R. This was repeated for different values of F from 0 to 1. The values of w, v, K and S were selected to minimize the RMS deviation between the model and the data simultaneously for R_i vs F, R_p vs F, and the overall R vs F.

Chapter 3: Behavior of halftones printed on EP printers

This section discusses the observed behavior of the printed halftones on both 600 dpi and 300 dpi EP printers. In the first subsection the histogram characteristics of these samples are discussed. When histograms of Floyd-Steinberg halftone patterns are observed, they differ significantly from the ideal halftone system behavior given by the Murray-Davies equation (2.1). The causes for this phenomenon are discussed in the following subsection. The last subsection contains results of applying the halftone model described in section 2.3.4 to characterize the behavior of the two printing systems chosen for this study

3.1 Tone behavior of halftones in histograms

The quality of printed halftone images is largely controlled by the spatial distribution of gray levels within the halftone structure. The distribution of the gray levels in printed halftones can be observed in the histogram of images captured using a CCD camera with microscopic optics. In our case, the histograms contain data

with reflectance values from 0 to 1. The histogram gives information on the fraction of total pixels in the captured image of that particular reflectance value (note: pixels referred in this statement are the pixels of the image through a digital camara and not of the original image that was printed). The histogram is useful for measuring specific attributes for microdensitometric analysis. Commonly applied metrics include the halftone dot area fraction, F, the mean reflectance of the paper between the halftone dots, R_p, and the mean reflectance of the dots, R_i. The procedure for measuring these metrics are described in detail in Appendix A, section A.1.

If we consider the histogram of the ideal halftone system (a system that obeys Murray-Davies Model, equation 2.1), its total pixel population should be localized at two specific points in the histogram: colorant reflectance R_i and paper reflectance R_p. Two examples of such a system are shown in Figure 3.1 and 3.2. These are halftone images of nominally uniform tone patches of constant reflectance. The first image has an average reflection of 0.75 and the second has average reflection of 0.5. By increasing the number of black dots, the fraction of the total area covered by colorant is increased, which results in a lower reflectance of that area of the print. Thus, increase in area fraction of the dots causes an increased

pixel population at R_i and a corresponding decrease in population at R_p.

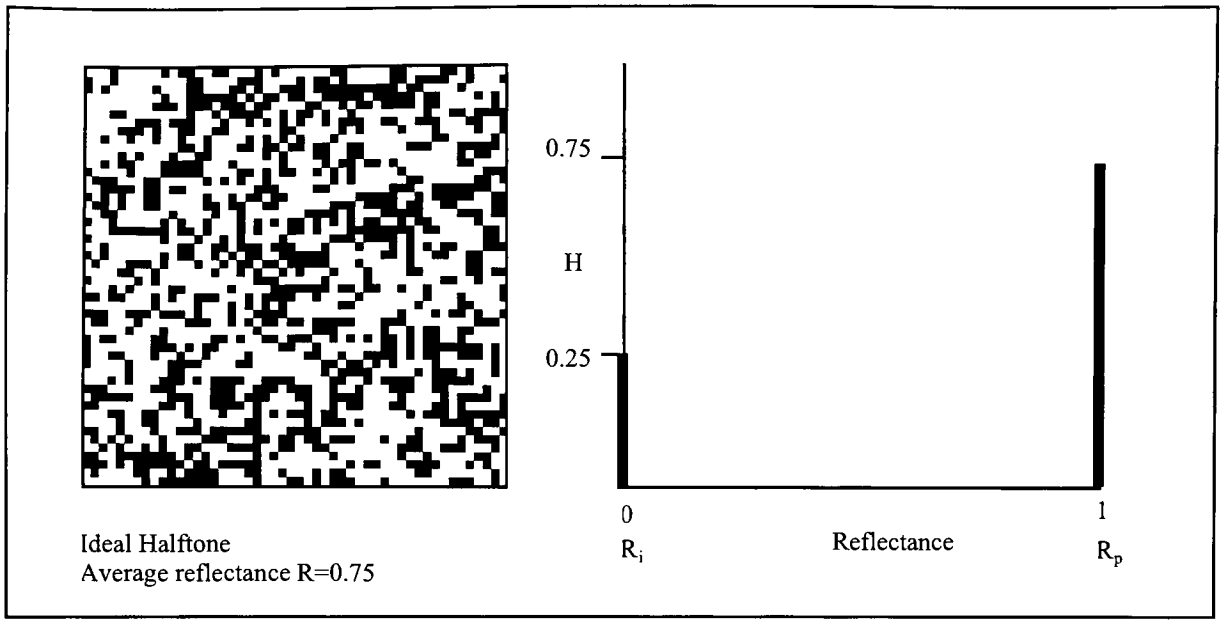

Figure 3.1: Image and histogram of an ideal halftone system

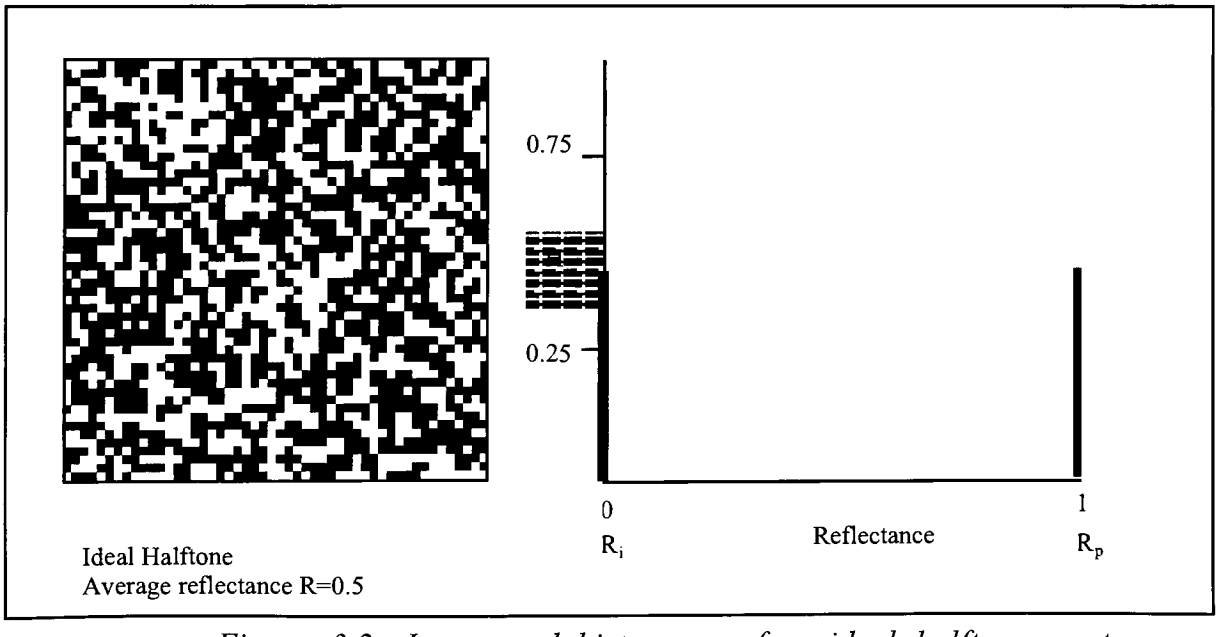

Figure 3.2: Image and histogram of an ideal halftone system population H vs. R on right

Consider the histogram of an ideal continuous tone image of a single tone. The total pixel population in a histogram would be situated at a single reflectance value, at the reflectance of the image, R. As the reflectance of the image changes, the population would move to the new reflectance value.

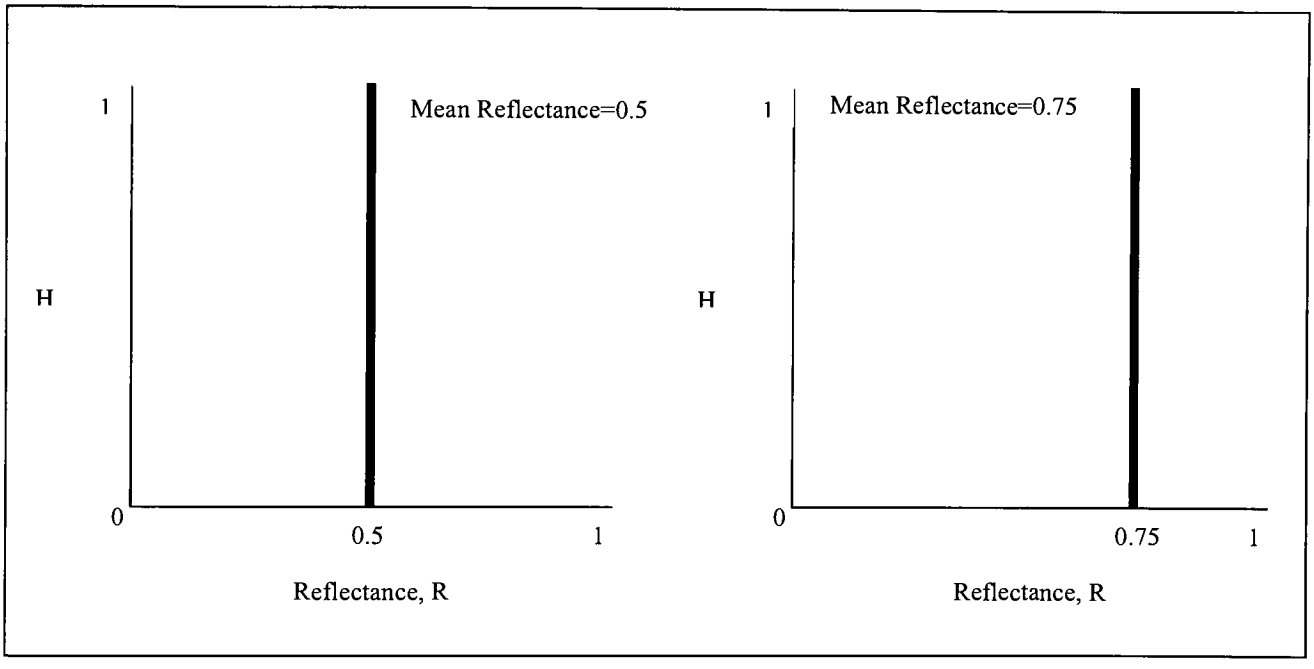

Figure 3.3: Histograms of ideal continuous tone system, at R=0.5 and R=0.75

To summarize the differences in the histogram behavior of both ideal halftone and continuous tone systems: in an ideal halftone system, changing F causes a change in the pixel

populations at R_i and R_p, whereas in an ideal continuous tone system the pixel population moves along the R axis.

The histograms of real systems do not have tightly populated, bimodal distributions. Due to local image variations (noise), the physical spread of the edges of halftone dots, and the optical scattering of light in the paper, the printed halftones have rather broad population distributions. Two examples of such histograms are shown in Figures 3.4 and 3.6 for samples printed on a 300-dpi EP printer using a Floyd-Steinberg halftoning algorithm. An increase in F_n (nominal dot fraction sent to the printer) results in an increase in the pixel population of the lower R distribution and a decrease in the higher R distribution. This is a characteristic of an ideal halftone system. However, the reflectance values at which the two local maxima occur change with the change in F_n. Thus the real system shown in figures 3.4 and 3.6, demonstrates characteristics of both an ideal halftone and a continuous tone system.

Histograms of samples printed using Floyd-Steinberg with a 600-dpi printer are shown in figures 3.5 and 3.7. The dots are visible and easily distinguishable from surrounding paper in these images. Unlike the histograms of the 300-dpi system, these histograms do not have two distinct populations. Rather, there is

one histogram maximum and a broad, asymmetrical distribution. As F_n is changed, the value of R at the peak changes. This behavior is more typical of a continuous tone system.

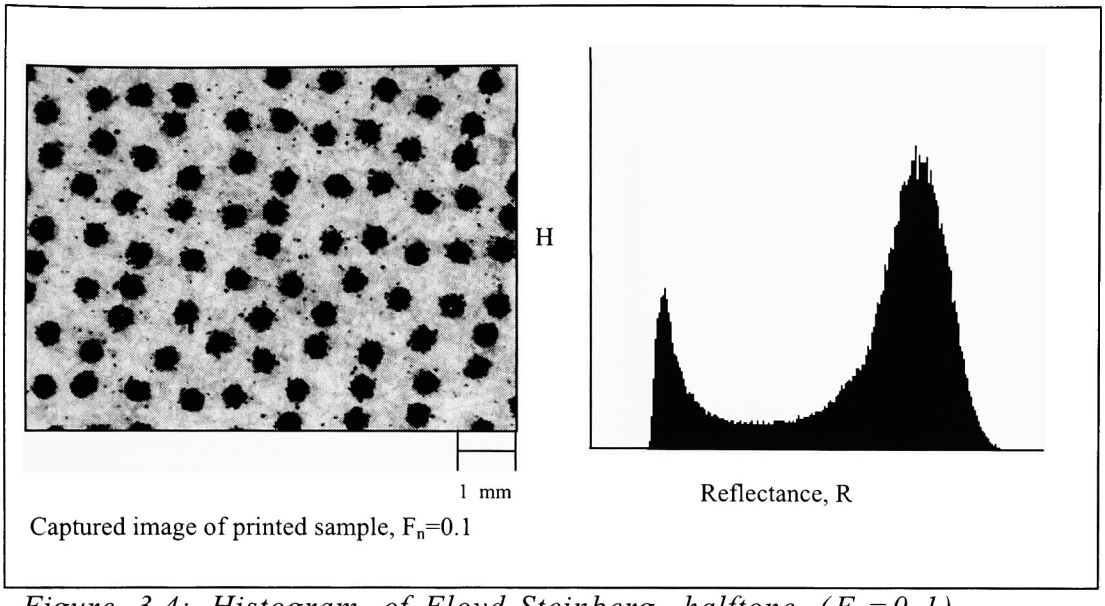

Figure 3.4: Histogram of Floyd-Steinberg halftone (F_n=0.1) printed on 300 dpi EP printer

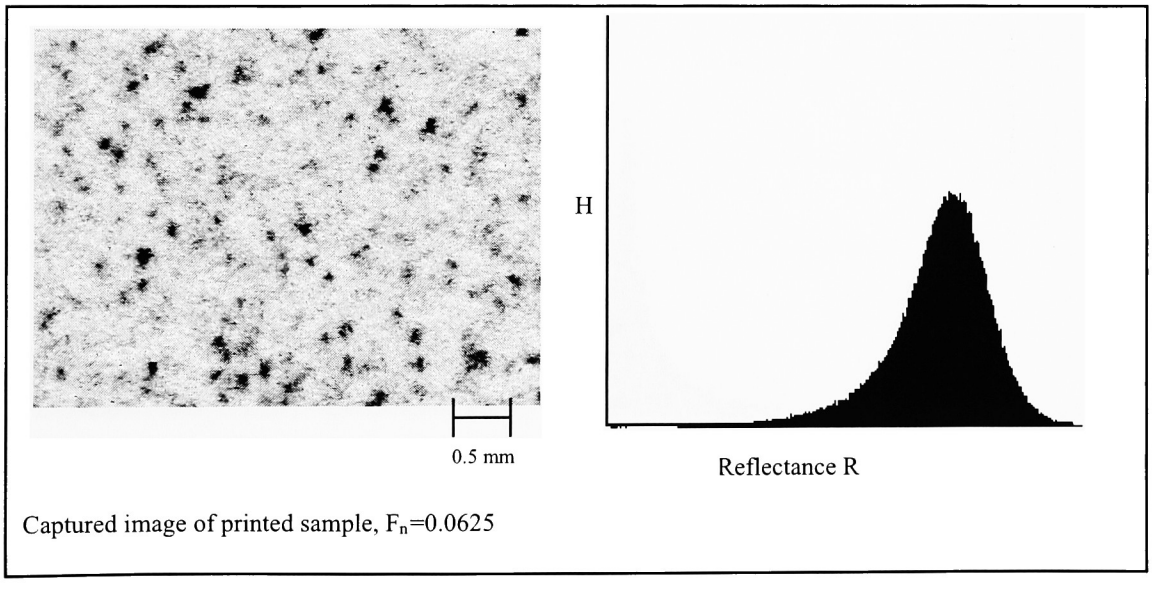

Figure 3.5: Histogram of a Floyd-Steinberg halftone printed on a 600 dpi printer, F_n =0.0625

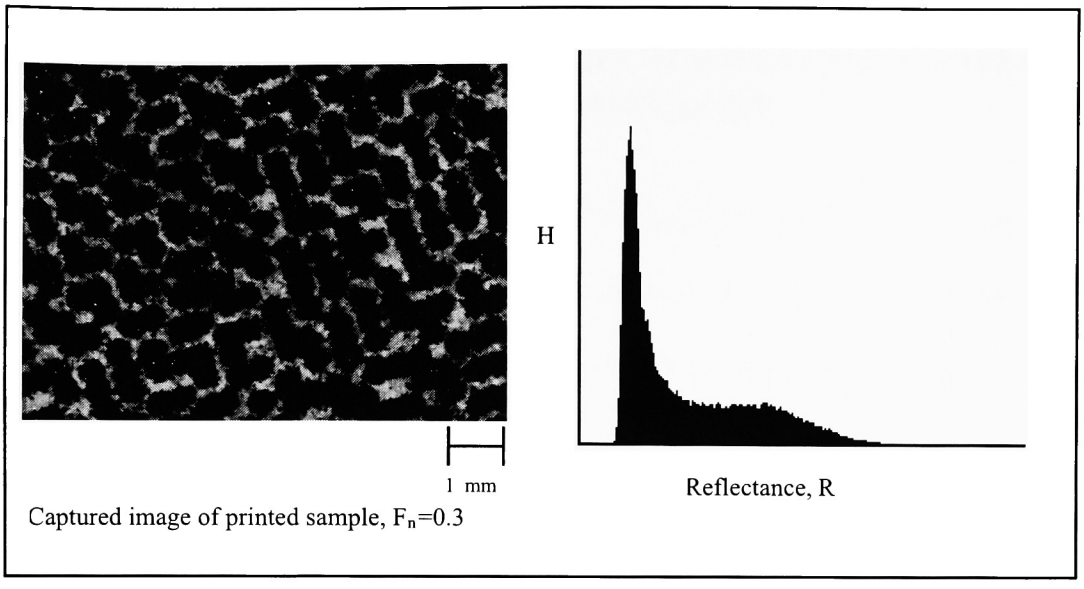

Figure 3.6: Histogram of Floyd-Steinberg halftone (F_n =0.3) printed on 300 dpi EP printer

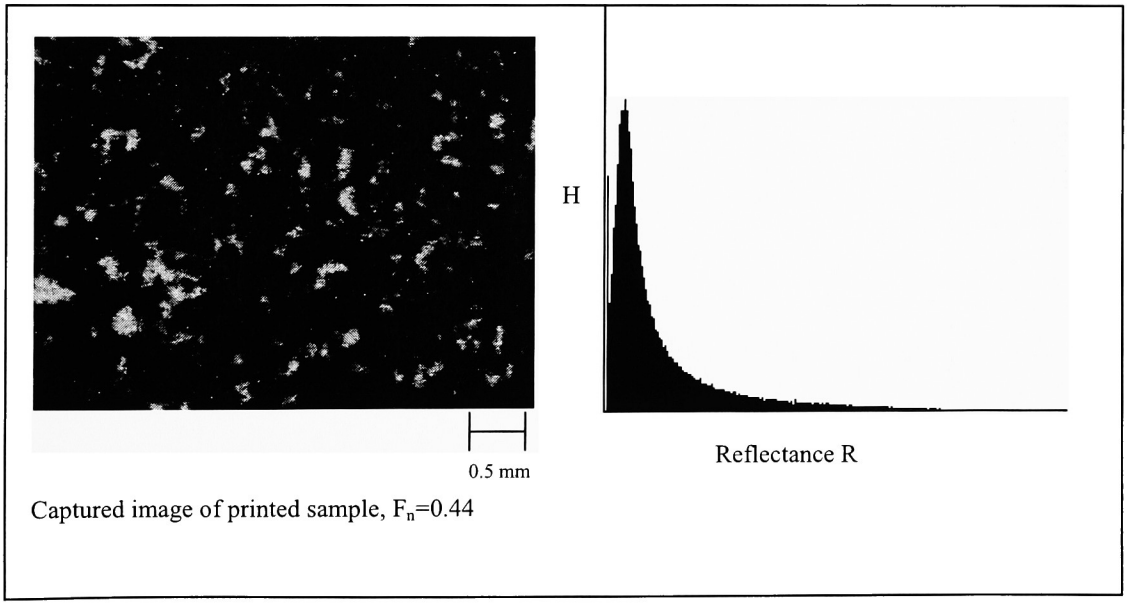

Figure 3.7: Histogram of a Floyd-Steinberg halftone printed on a 600 dpi printer, F_n =0.44

3.2 Observation of printed images at microscopic level and point spread function of non-coated paper

A comparison of microscopic views of samples printed with 600 dpi and 300 dpi EP printers is shown in figure 3.8. The samples printed on the 300 dpi printer have well formed dots. Toner particles are scattered, but the amount of scattering is not as significant as it is for the 600dpi printer samples. The dots formed by the 600dpi printer are not well defined. The dots do not exist as a continuous toner layer. Rather, we see clusters of toner particles. The edge of the dot in such a case is not as well defined as for the samples from the 300dpi printer.

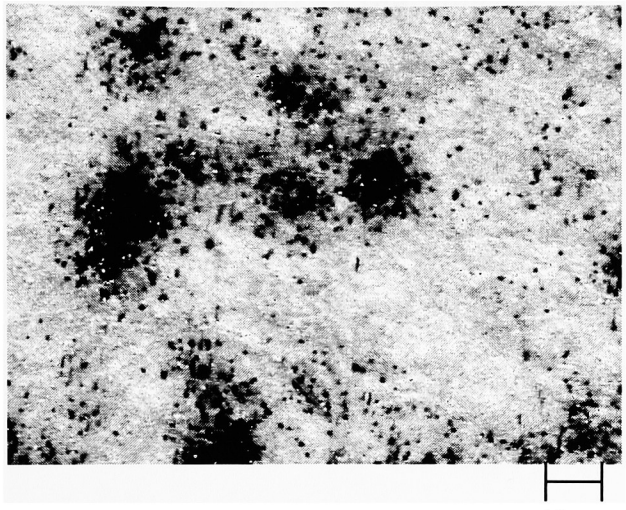

Sample printed on 600dpi, Fn=0.20

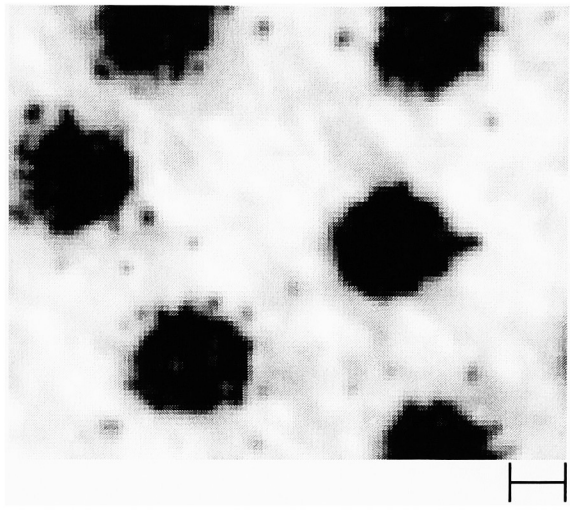

Sample printed on 300dpi, Fn=0.20

Figure 3.8:Microscopic view of print samples printed on 600dpi and 300 dpi electrophotographic printer (please note that magnification is not same for both image

$$\text{Size of the dot (in mm)} = \frac{25.4}{\text{Adderessibility of the printer}} \qquad (3.1)$$

The average size of a printed dot can be estimated by equation (3.1). This equation does not account for dot gain. The average size of a dot for a 600dpi printer calculated from this equation is 42μm and for 300 dpi, it is 84μm.

It was shown in the past that the lateral scattering of light in paper has a major impact on the tone reproduction behavior of the electrophotographic systems (Huntsman, 1987). A useful metric of

lateral scatter is the modulation transfer function, MTF, defined as the modulus of the Fourier transform of the line spread function. This metric describes the magnitude of light scatter in paper in terms of spatial frequency, ω, in units of inverse distance (mm^{-1}). The point spread function, PSF, is also found to be a useful metric to measure scatter distances in the paper.

$$MTF = e^{(2\pi k\omega)^2} \tag{3.2}$$

$$PSF = e^{\left(\frac{r}{2k}\right)^2} \tag{3.3}$$

The MTF of the non-coated paper used in this study can be modeled by equation (3.2) (Dainty-Shaw, 1974). Parameter *k* in equation (3.2) is empirical and r is the radial distance. The point spread function, PSF, for this MTF is given by Equation (3.3). This PSF has gaussian-like behavior and therefore the value of r where PSF equals to 0.5 is the average distance that light scatters in paper before it is absorbed or reflected. Experimentally, at a frequency of ω = 2 cycles/mm, the MTF of the paper is 0.5 (Arney-Arney-Katsube-Engeldrum, 1996). By substituting these values in equation

(3.2), a value of k=0.066mm is calculated. Using this value of *k* and using a value of PSF=0.5, a value of r =0.11 mm can be estimated.

In other words, the average distance light scatters latterly within the paper before returning to the surface as reflected light is around 100μm. This is about the size of a dot printed at 300 dpi (84μm) and twice the size of the 600 dpi dot (42μm). Therefore, most photons entering the image printed at 600 dpi will encounter more than one area of addressability. This is analogous to silver halide systems. The silver grains are discretely distributed in the image as illustrated in Figure 3.9. The size of the grains are so small that the silver halide systems have always been modeled as continuous tone systems. Therefore, it seems reasonable to explore the potential utility of modeling the 600 dpi system as a continuous tone system.

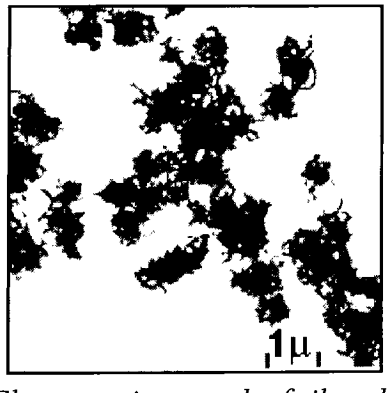

Figure 3.9: Electron micrograph of silver-halide system.
(Please note the difference of magnification between figures 3.8 and 3.9)

Chapter 4: Continuous Tone Model

Discussion of points in chapter 3:

- The histograms of microdensitometry images of Floyd-Steinberg halftones printed on a 600dpi EP printer do not have a typical bimodal distribution. The dots are radiometrically indistinguishable from the paper between them. The pixel population is centered at one reflectance value, and the reflectance value at the center changes as F_n changes. This is similar to behavior typically seen in histograms of continuous tone systems.
- This might be caused due to the fact that the average size of the dot printed on the 600dpi printer is about the same as the average distance of light scattering in the paper. Therefore, the printed samples behave more like continuous tone systems even in microdensitometric images and in histograms.
- To apply most halftone models, the required printed dot area fraction F can be satisfactorily estimated from a bimodal histogram. Since the histograms of

Floyd-steinberg halftones printed on the 600dpi printer do not have two distinct populations, it is not possible simply to estimate F from the histograms.

These observations suggest it might be useful to apply a continuous tone model to characterize the tone-reproduction behavior of Floyd-Steinberg halftones printed on a 600dpi EP printer. Discussions of the models and their application to these images are made in the following sections. The models are also applied to other printing systems (lower resolution and clustered dot screening) considered in this work.

The well-known continuous tone models are the Beer-Lambert model and the Kubelka-Munk model (Berns, 2000). The Beer-Lambert model makes an assumption about the behavior of the imaging system that makes it simpler than the Kubelka-Munk model. To begin the continuous tone model, we will begin with the Beer-Lambert model.

4.1 Beer-Lambert Transmittance

Consider a system that absorbs light but does not scatter it. This is well known as the "Beer-Lambert" phenomenon, shown in figure (4.1). I_0 is the irradiance entering the image layer, and I is the irradiance leaving the imaging layer.

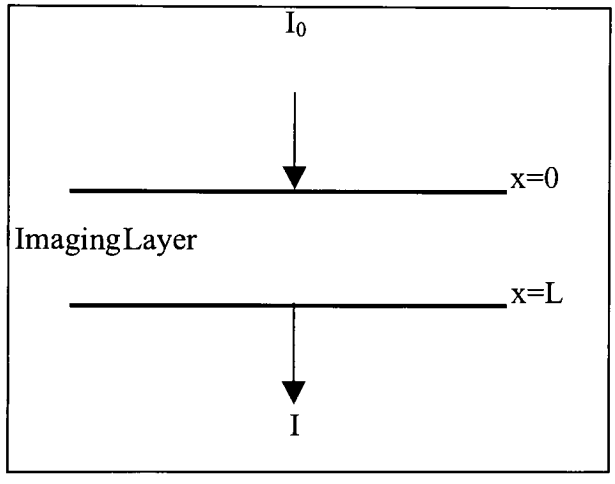

Figure 4.1: The Beer- Lambert phenomenon

The Beer-Lambert model can be described as follows. The rate at which irradiance decreases with depth, -dI/dx, is proportional to the magnitude of irradiance, I(x), at depth x. This is written mathematically as equation (4.1), where K' is a constant of proportionality.

$$-\frac{dI(x)}{dx} = K' \cdot I(x) \tag{4.1}$$

Similarly, the rate of change in irradiance due to changes in concentration of colorant in the imaging layer is written as equation (4.2), where K" is another constant of proportionality.

$$-\frac{dI(x)}{dc} = K'' \cdot I(c) \tag{4.2}$$

Equations (4.1) and 4.2) can be combined into a single first-order differential equation, and integration with the boundary condition of $I = I_0$ at $x = 0$ and $I = I_0$ at $c = 0$ gives equation 4.3 for the overall image layer of thickness L and colorant concentration c. (Berns, 2000).

$$I = I_0 e^{-\varepsilon c L} \tag{4.3}$$

The transmittance of the imaging layer, T, is defined as ratio of entering and leaving irradiance, as given in equation (4.4). And the transmission density of the imaging layer is defined by equation (4.5). In the equation (4.5), ε is the extinction coefficient of the colorant material of the imaging layer in units of grams·mm^{-2}, c is

concentration of colorant in grams/mm^3, and L is thickness of imaging layer in mm.

$$T = I/I_0 \tag{4.4}$$

$$D_T = -\log(T) = \varepsilon \cdot c \cdot L \tag{4.5}$$

4.2 Beer-Lambert Reflectance

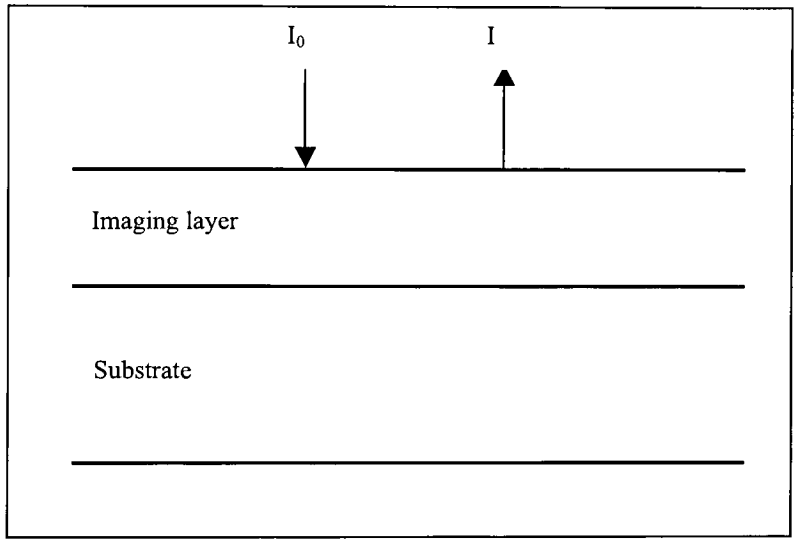

Figure4.2:Beer-Lambert Phenomenon in the Imaging Layer applied on the Substrate

Now consider the imaging layer applied on a substrate (such as paper) with Lambertian diffuse reflectance of R_g, as illustrated in figure 4.2. The reflectance of the imaging layer, R, is defined at the ratio of the reflected irradiance to the incident irradiance, as given by equation (4.7). The reflective density, D_R, of this system

is defined as equation (4.8). The reflectance of the system, R, is related to the transmittance of the layer, T, and the reflectance of the substrate, R_g, by equation 4.9. Let D_g=-log(R_g) and D_T=-log(T), and we have equation (4.10).

$$R = I/I_0 \tag{4.7}$$

$$D_R = -\log(R) \tag{4.8}$$

$$R = T^2 \cdot R_g \tag{4.9}$$

$$D_R = D_g + 2D_T \tag{4.10}$$

The mass of colorant per unit area is the coverage, C, and the coverage is related to the layer density by $D_T = \varepsilon C$. This allows us to write the reflection density of the image, D_R, as a function of colorant coverage, equation (4.11). Density is therefore expected to increase linearly with coverage for a Beer-Lambert image. Note also, as illustrated in Figure 4.3, that the curve plotted as R versus C is concave. This behavior is reminiscent of dot gain phenomena.

$$D_R = D_g + 2\varepsilon \cdot C \tag{4.11}$$

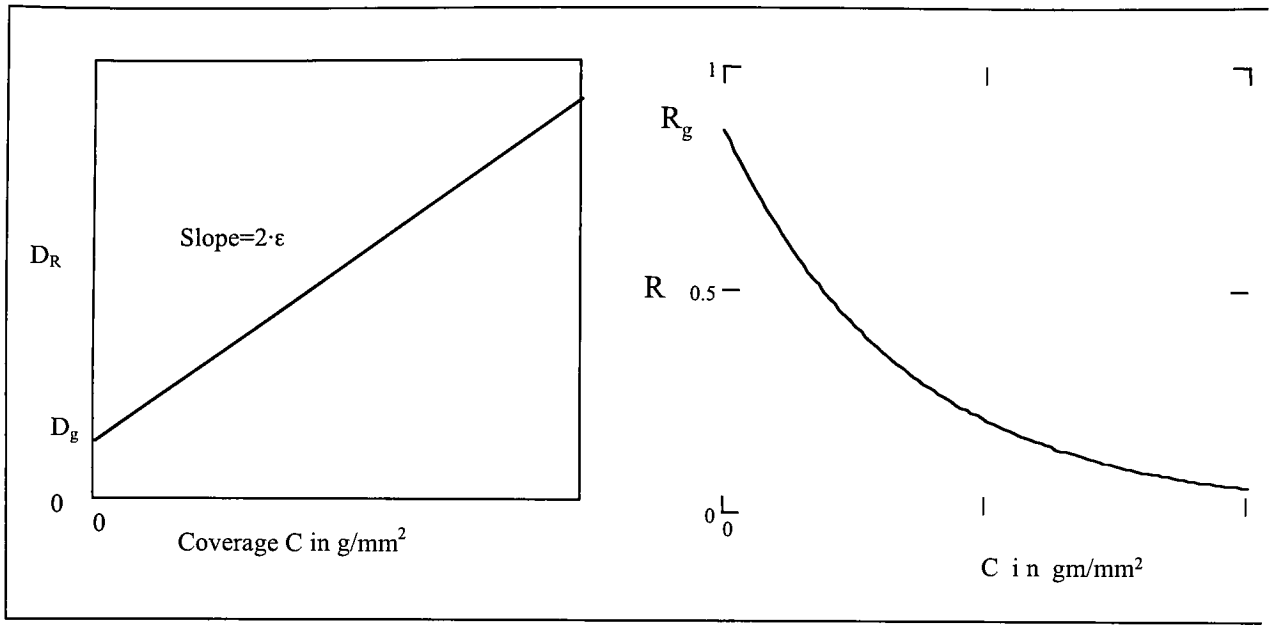

Figure 4.3: D_R vs C and R vs. C curves of Beer-Lambert model

4.3 Applying the Beer-Lambert Model to a Halftone

The Beer-Lambert model as expressed in equation (4.11) relates the absorption of the light in the imaging layer to the coverage of colorant in the image layer. In order to apply this Beer-Lambert model to a halftone, we assume the halftone behaves as a uniform distribution of colorant. For halftones of high spatial frequency in which the distance of light scattering is large relative to dot sizes, this approximation seems reasonable. In order to

compare the Beer-Lambert model to printed halftones, samples were printed on the 600dpi printer. The continuous tone model assumes that the nominal dot area fractions, F_n, sent to the printer controls the mean coverage of colorant, C, delivered to the printer. In an ideal halftone system, C is directly proportional to F_n. To apply the Beer-Lambert model as written in equation (4.11), it is necessary to establish a relation between the coverage C and the printer command, F_n. This relationship was found experimentally by a gravimetric analysis. The details of the gravimetric analysis are explained in the next section. The coverage was measured experimentally by weighing paper samples before and after printing. Samples were equilibrated at the lab RH and temperature before weighing, and the RH and temperature of the lab remained constant during the project. The increased weight from printing was divided by the area of the printed sample to obtain the measured coverage, C. The value of C was measured in this way for samples printed at different value of nominal dot area fraction, F_n. This analysis was carried out for black toner printed on plain office copy paper with both a 300 dpi laser printer and a 600 dpi printer. The same Floyd-Steinberg halftone algorithm was used in both experiments. Figure (4.4) shows the results.

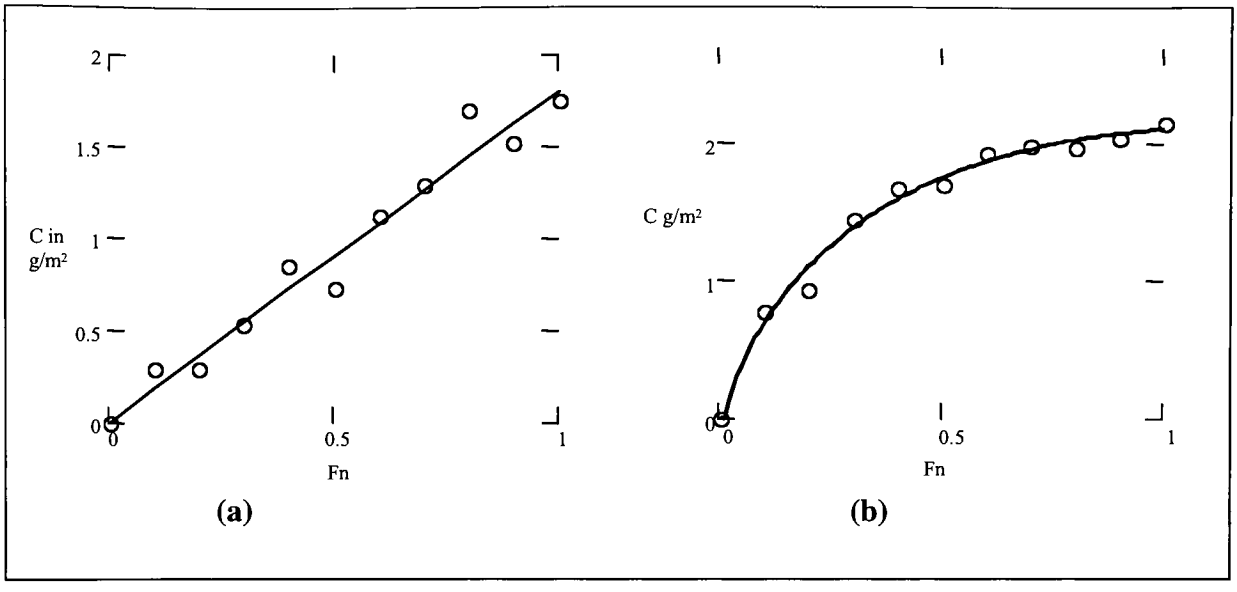

Figure4.4: Result of Gravimatric analysis
(a) 600dpi printer modeled by $C=1.8F_n$
(b) 300 dpi Printer modeled using a polynomial fit
$C=-3.1F_n+9.6\ F_n^{1/2}-4.4\ F_n^{1/3}$

The solid lines in Figure 4.4 (a) and (b) are equations (4.12) and (4.13) respectively. These equations are empirical functions chosen statistically to model the data.

$$C = 1.8F_n \tag{4.12}$$

$$C=-3.1F_n + 9.6F_n^{1/2} \quad 4.4F_n^{1/3} \tag{4.13}$$

By applying equation (4.12) or (4.13) to the Beer-Lambert of equation(4.11), we have a simple model for reflectance, R, versus F_n. Two constants, D_g and ε, must be known in order to apply the model. The value of D_g is the reflection density of the unprinted

paper and is easily measured. The value of ε can be adjusted to fit the model for R vs F_n to experimental data. Figure 4.5 shows the results for the 300 dpi and the 600 dpi printer using Floyd-Steinberg.

The comparison between the simple Beer-Lambert model and the experimental data shown in Figure 4.5 was made with values of ε = 0.3 and 0.5 m^2/g. No value of ε was found to provide a high quality fit between the model and the data for either the 300 or the 600 dpi printer. However, it is interesting to compare the Beer-Lambert model to the simple halftone model of Murray-Davies (dotted lines in Fig. 4.5, equation 2.1). It is evident that the Murray-Davies model would have to be modified quite significantly in order to fit the data. The simple Beer-Lambert model appears to be a much closer approximation that the Murray-Davies model and may require far less modification than Murray-Davies in order to rationalize the data. Thus, modifications to the simple Beer-Lambert model were investigated as described below.

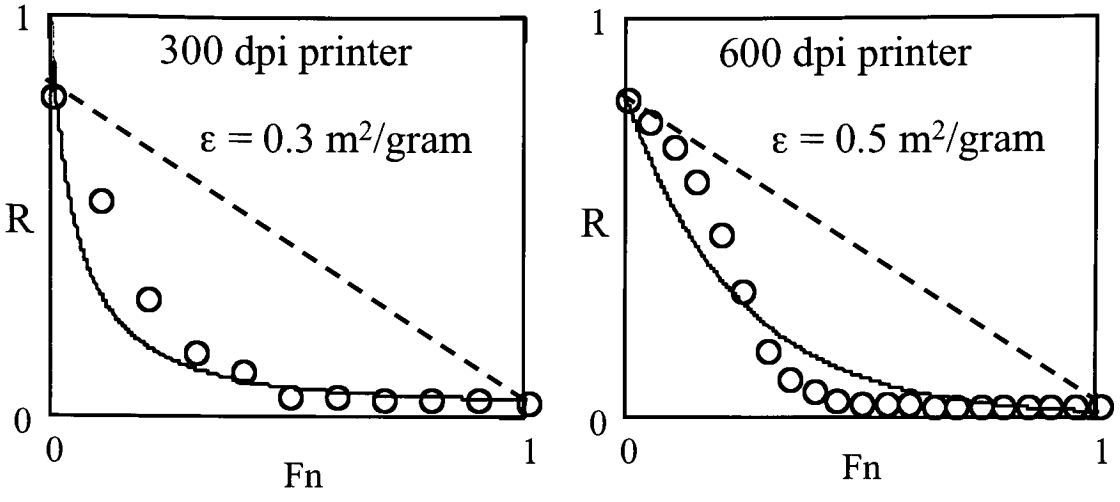

Figure 4.5: *Reflectance versus nominal dot area fraction for Floyd-Steinberg halftones printed with a 300 dpi printer and a 600 dpi printer. Measured data is* O, *the Beer-Lambert model is* ———, *and the Murray-Davies model is* ------.

4.4 Kubelka-Munk Model

The first modification to the simple Beer-Lambert model considered in this project was to include optical scattering in the colorant layer. In other words, we assume there may be some significant scattering of light within the toner used in the laser printers. The printed halftone image was again modeled as a contiguous image layer, and scattering was modeled by applying the Kubelka-Munk theory, as shown in Figure 4.6. Kubelka and Munk suggested that the scattering phenomenon, like the absorption phenomenon, is a first order phenomenon (Kubelka-Munk, 1931).

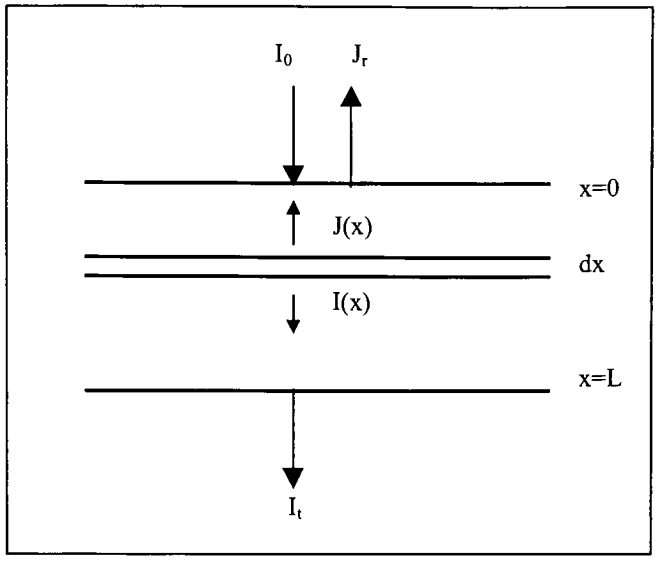

Figure 4.6:Kubelka-Munk Theory

Consider a small layer within the imaging layer at distance x from the top and of thickness dx. The flux of light in the downward direction is called I, and the flux in the upward direction is called J. Both I and J are changed as a function of depth, x, in the layer by first order absorption and scattering as described in equations (4.14) and (4.15). K and S are the first order absorption and scattering constants in units of mm^{-1}. The value of K is related to the Beer-Lambert extinction coefficient, ε, by equation (4.16). Note that c = C/L, where c is concentration in g/m^3 and C is coverage in g/m^2.

$$dI = -KIdx - SIdx + SJdx \qquad (4.14)$$

$$dJ = -KJdx - SJdx + SIdx \qquad (4.15)$$

$$K = 2.303 \cdot \varepsilon \cdot c \tag{4.16}$$

$$T = I_t / I_0 \tag{4.17}$$

$$R = J_r / I_0 \tag{4.18}$$

I_t is the downward flux leaving the bottom of the material at x = L, and J_r is upward flux leaving the surface of the material at x = 0. With these boundary conditions, and the definitions of transmittance and reflectance given in equations (4.17) and (4.18), the Kubelka-Munk differential equations can be solved to give algebraic expressions for $R=f_1(S,K,L,R_g)$ and $T=f_2(S,K,L)$. The general solutions for the functions f_1 and f_2 can be expressed as follows.

$$a = \frac{(S + K)}{S} \tag{4.19}$$

$$b = \sqrt{a^2 - 1} \tag{4.20}$$

$$R = \frac{1 - Rg[a - b \cdot \coth(bSL)]}{a - Rg + b \cdot \coth(bSL)} \tag{4.21}$$

$$T = \frac{b}{a \cdot \sinh(bSL) + b \cdot \cosh(bSL)} \tag{4.22}$$

The parameters in the Kubelka-Munk model are the same R_g and ε of the Beer-Lambert model. In addition, the Kubelka-Munk model has a scattering coefficient, S, and a thickness term, L. It can be shown that in the limit as $S \rightarrow 0$, the Kubelka-Munk model is

identical to the Beer-Lambert model. In this case, the model for R versus coverage, C, is independent of L. If the value of S is significant, then both S and L must be included as independent parameters in the model.

Figure 4.7 shows the experimental data for the 600 dpi printer both as reflectance, R, versus F_n and reflection density, D, versus F_n. The dotted line in D vs F_n is a straight line characteristic of the Beer-Lambert model. The solid line was modeled with the Kubelka-Munk functions using R_g=0.8, ε=1.0 m^2/g, S = 20 mm^{-1}, and L = 0.01 mm. This illustrates the typical effect of scattering in which the linear increase in density bends over at higher density.

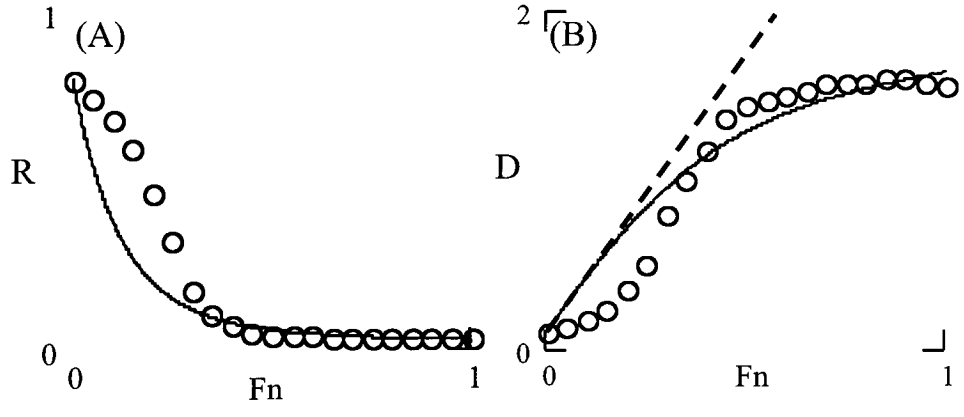

Figure 4.7: *R versus F_n and D versus F_n for the 600 dpi printer. Measured data is* O, *the Kubelka-Munk model is* ——, *and the Beer-Lambert model is* -------

The Kubelka-Munk model with S>0 provides a potential rational for the shape of the D vs F_n curve at high density. However, the model was found to be unable to rationalize the data for density values below 1.0, regardless of the combination of parameters chosen for the model. Thus, it is evident that some other effect besides. or in addition to, scattering must be causing the variation between the continuous tone model and the actual data.

4.5 Spatial Efficiency Function

The failure of the ideal halftone model of Murray-Davies is often called the dot-gain effect. This is because the image is darker than predicted by Murray-Davies. In other words, the probability that the ink will absorb light is higher than anticipated. The reasons for this increased absorption probability are associated with spatial attributes of the halftone dots. A physical spreading out of the halftone dots (physical dot-gain) increases the absorption efficiency of the ink in terms of numbers of photons absorbed per mass of ink. The second effect is an optical effect of light scattering within the substrate paper. This spatial effect also increases the absorption efficiency of the ink.

Inspection of the Kubelka-Munk and Beer-Lambert models shown in Figure 4.7 (B) significantly over estimate the darkening of the image for density values below 1. In other words, it appears that the continuous tone model over-compensates for the dot gain effect. One might call this effect of over-estimating the darkness of the image an "ink anti-gain" effect. The light absorption efficiency of the ink is less than anticipated based on the ideal continuous tone model.

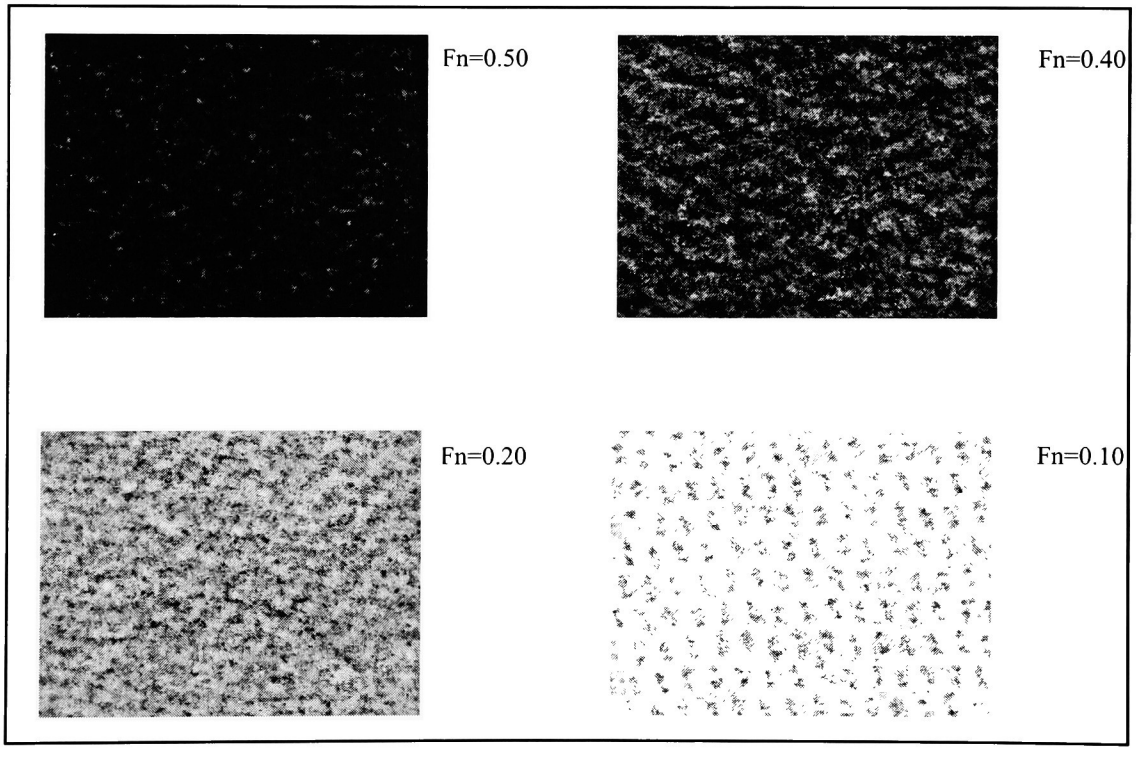

Figure 4.8: Microdensitometry images of Floyd-Steinberg halftones printed on 600 dpi printer at several values of Fn.

The concept of an ink anti-gain effect is illustrated in Figure 4.9. If the ink in a continuous tone image layer is segmented spatially into regions of high and low coverage, maintaining a constant amount of ink, the image will be lighter than predicted by the continuous layer model. In other words, the ink will absorb less light per mass of ink. The magnitude of the effect will vary depending on the amount of clustering of ink that occurs, and this in turn will cause it to vary as a function of the nominal dot area fraction, F_n. Thus, in order to model the ink anti-gain effect, we must model the absorption probability, ε, as a function of F_n.

4.5.1 An Empirical Function

One might attempt to model ε versus F_n based on fundamental theory. The theory would combine dot gain with the basic theory of light scattering in paper that has been used to model halftone systems. However, for this project the relationship between ε and F_n was modeled empirically. The model begins with a value of ε at 100% coverage ($F_n = 1$). This is called ε_o and is a characteristic of the ink. The value of ε decreases as F_n increases, and a number of

empirical functions, $f(F_n)$, were explored to describe this effect. The function $f(F_n)$ that seemed to provide the

$$\varepsilon(F_n) = \varepsilon_o \cdot f(F_n) \tag{4.23}$$

best overall performance, as will be shown below, was the sigmoid function of equation (4.24), illustrated in Figure 4.8. The constants

$$f(F_n) = \frac{1}{1+\exp\{-k(F_n - F_c)\}} \tag{4.24}$$

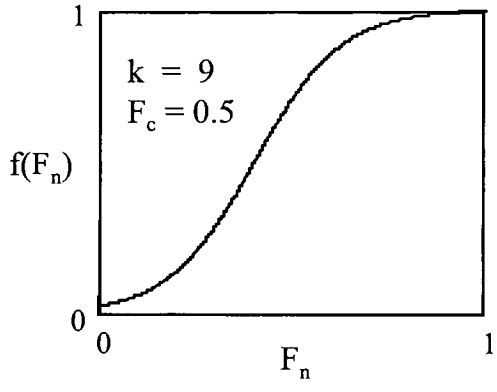

Figure 4.8: *Spatial efficiency function used to modify the continuous tone model.*

k and F_c are two arbitrary constants chosen to fit experimental data. In the current project, the physical significance of these two constants was not explored.

4.5.2 The Beer-Lambert Model Modified with the Spatial Absorption Function

The Beer-Lambert model was modified to include the spatial absorption function. The simple Beer-Lambert model used a single arbitrary constant, ε. The spatially modified model uses three arbitrary constants, ε_o, k, and F_c. By adjusting these constants, the Beer-Lambert model can be made to fit the low density portion of the experimental data, as illustrated for the 600 dpi printer in Figure 4.9.

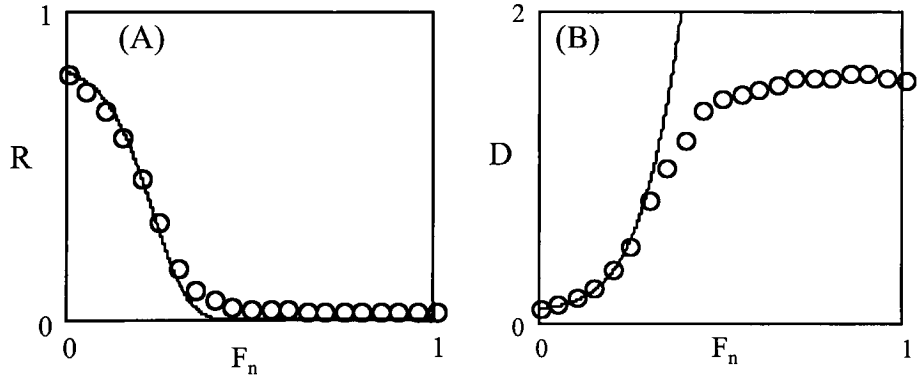

Figure 4.9: *R versus F_n and D versus F_n for the 600 dpi printer. Measured data is O, and the Beer-Lambert model with a spatially varying ε is ——. Fit parameters are ε_o = 5 m^2/g, k = 9, and F_c=0.5*

The fit between the data for the 600 dpi printer and the model in Figure 4.9 is good for density values below 1.0. The failure of

the model for D > 1 suggests a significant contribution from a scattering coefficient S > 0 in the toner.

4.5.3 The Kubelka-Munk Model Modified with the Spatial Absorption Function

The Kubelka-Munk model can be modified to account for a spatially varying absorption coefficient exactly as was done for the Beer-Lambert model. The value of F_n is varied over the range $0<F_n<1$, and at each value of F_n a value of C is calculated with either equation 4.12 or 4.13, and also a value of ε is calculated from equation 4.23. The remainder of the Kubelka-Munk model is applied exactly as described in section 4.4.

The variables one can adjust in this model are ε_o, S, L, k, and F_c. Figure 4.10 shows the data and model. It is significant to point out that the model was fit to the data using the same values of ε_o, S, k, and F_c. Only the values of L are different, and it seems reasonable that the toner pile height with the two printers might indeed be different.

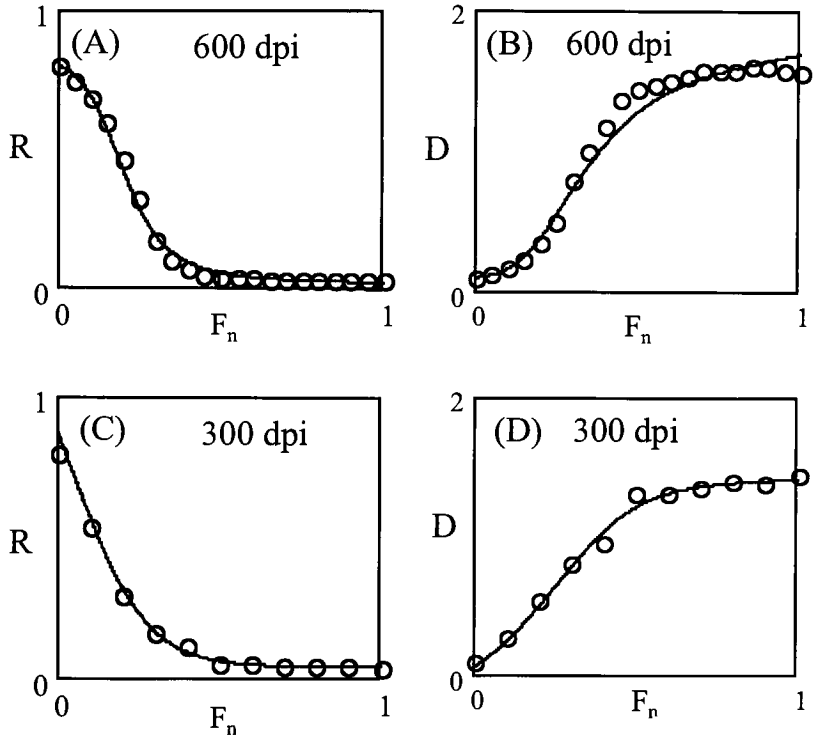

Figure 4.10: *R versus F_n and D versus F_n for the 300 and 600 dpi printers. Measured data is O, and the Kubelka-Munk model with a spatially varying ε is ——. Fit parameters are ε_o = 5 m^2/g, k = 9, and F_c = 0.4, S=90mm^{-1}. L = 0.01 mm for the 600 dpi printer, and L = 0.023 mm for the 300dpi printer.*

4.6 Relating the Printing Resolution to Spatial Efficiency Function

In order to understand the factors influencing our ink anti-gain model, represented quantitatively by the spatial efficiency function, $f(F_n)$ in equation 4.23, we printed and modeled halftone images with a wide variety of spatial frequency characteristics. In addition to the 600 dpi printer, we used a 300 dpi color laserjet printer. Both printers were manufactured by Hewlet-Packard and were purchased commercially Gray ramps were printed with both black toner and cyan toner using both a clustered dot halftone algorithm and a Floyd-Steinberg algorithm. The clustered dots were printed at 120 LPI with the 600 dpi printer, and at 60 LPI with the 300 dpi printer. A summary of the eight gray ramps is shown in Table 4.1. The "A" parameter is described below.

Printer dpi	Halftone Pattern	Toner	Dot Pitch lines/inch	F_c	k	A	ε_o	S mm^{-1}	L mm
600	F-S	Black	600 LPI	0.40	9	0.60	5.0	90	0.01
600	CL	Black	120 LPI	0.50	6	0.50	4.3	90	0.01
600	F-S	Cyan	600 LPI	0.20	9	0.78	0.48	0	--
600	CL	Cyan	120 LPI	0.33	5	0.64	0.36	0	--
300	F-S	Black	300 LPI	0.40	9	0.60	5.0	90	0.23
300	CL	Black	60 LPI	0.80	5	0.26	5.0	90	0.23
300	F-S	Cyan	300 LPI	0.10	15	0.89	0.34	0	--
300	CL	Cyan	60 LPI	0.23	5	0.72	0.34	0	--

Table 4.1: *Characteristics of the samples included in the study. Printer dpi is addressability in dots per inch. F-S and CL are Floyd-Steinberg and Clustered dot respectively.*

The clustered dots were formed from 5x5 masks. Dot pitch in LPI is the closest possible distance between two printed dots. The remaining terms are defined in the text and equations.

Table 4.1 also shows the model parameters that were used to fit the experimental data. The parameter values were selected by visually judging the quality of fit between the model and the data. Figures4.11 and 4.12 show the agreement between the model and the data for R vs F_n.

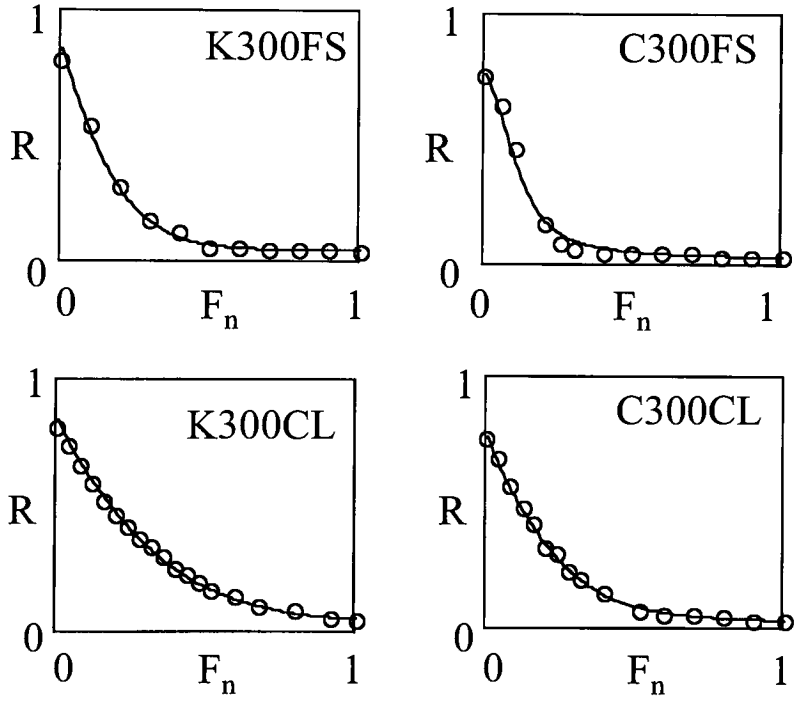

Figure 4.11: R vs Fn for the 300 dpi printer with black (K) and cyan (C) toner using Floyd-Steinberg (FS) and clustered dot (CL) halftoning. Circles are data points and solid lines are models.

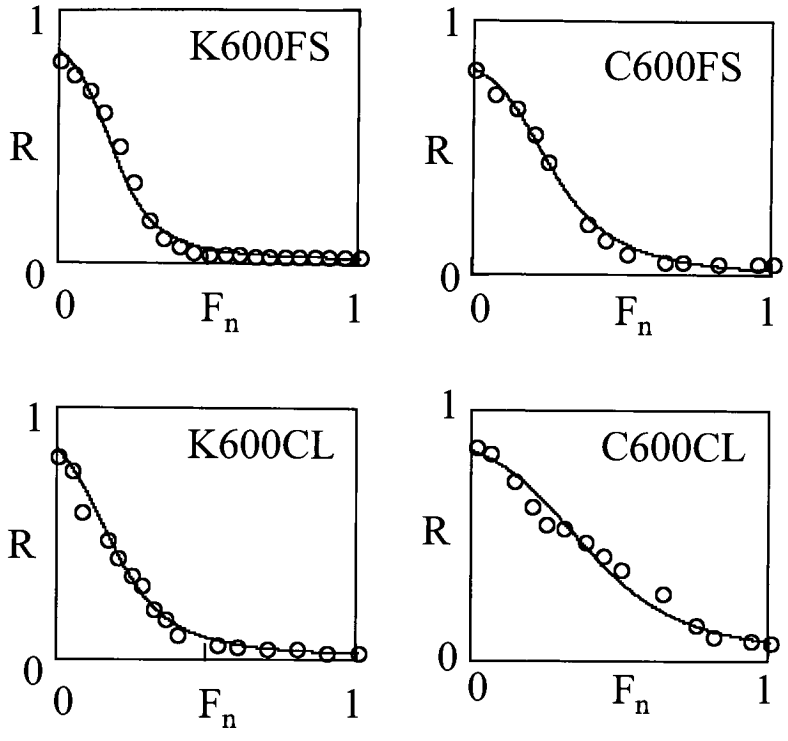

Figure 4.12: R vs Fn for the 600 dpi printer with black (K) and cyan (C) toner using Floyd-Steinberg (FS) and clustered dot (CL) halftoning. Circles are data points and solid lines are models.

4.6.1 The "A" Parameter

The spatial efficiency function of equation 4.23 contains a slope term, k, and a central position term, F_c. However, in order to compare the overall spatial efficiency of each system represented in Table 4.1, a single spatial efficiency metric was defined as shown in Figure 4.12. The area, A, under the curve is a measure of the efficiency with which the system uses the absorption coefficient of

the toner, ε_o. The value of A is in the range A = 0 for complete inefficiency to A = 1 for complete efficiency of use.

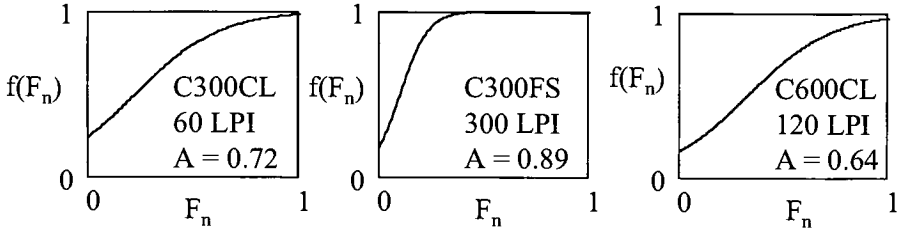

Figure 4.13 Efficiency functions used to fit three of the gray ramps in Figures 4.11 and 4.12. The A parameter is the area under the curves integrated over the range 0 < Fn < 1.

One would expect a value of A = 1 for a very high frequency halftone. This is because a very high frequency halftone suffers the maximum possible dot gain at all values of F_n, so ε does not change with F_n.

At the other extreme of very large halftone dots (very low frequency) there is no dot gain. Again the system shows no change in ε as a function of F_n, so A again should be 1.

For a spatial frequency at which the halftone shows the maximum dot gain effect, we also have the maximum ink anti-gain effect. In this case, we would expect ε to vary most greatly as a function of F_n. Figure 4.13 is a plot of the area factor, A, as a

function of the halftone frequency, expressed as the dot pitch in lines per inch, LPI, from Table 4.1. The result appears quite scattered, but the overall trend seems consistent with the expected minimum in A. Moreover, the minimum in A seems to be in the frequency range, ~100 to ~300 LPI, or ~4 to ~12 cycles/millimeter. The frequency at which the MTF of plain paper, used in this experiment, drops to 0.5 is about 6 cycles/millimeter, which in turn is the frequency at which one would expect the maximum optical dot gain.

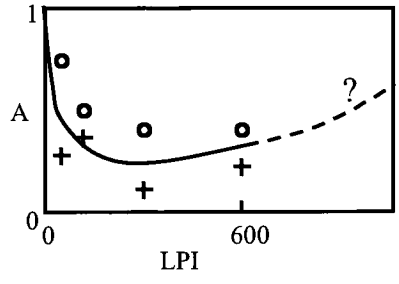

Figure 4.14: *Spatial efficiency factor, A, versus the dot pitch, LPI, for the black (+) toner data and the cyan (O) data.*

Chapter 5: Conclusion and Recommendations

Real-world halftone systems like those used in this study are neither ideal halftones nor ideal continuous tone systems. Traditionally, the tone reproduction behavior of an electrophotographic printing system is modeled by applying corrections to an ideal halftone model, as discussed in section 2.3.4. This seems reasonable since the algorithm used to control the delivery of toner is a halftone algorithm such as a clustered dot or a Floyd-Steinberg algorithm. The corrections generally applied are corrections that account for spatial effects called dot gain. These corrections are summarized in Table 5.1.

Corrections needed for an ideal halftone model:	**Corrections needed for an ideal continuous tone model:**
1. Physical Dot Gain effects 2. Optical Dot Gain (Yule-Nielsen Effect)	1. Ink Delivery Efficiency (Like Physical Dot Gain) 2. Spatial Absorption Efficiency (ink anti-gain)

Table 5.1: Variations from Ideal system

Also shown in Table 5.1 are the corrections required to make an ideal continuous tone model correctly describe a real world system. The continuous tone model uses a correction that is essentially the reverse of the optical dot gain correction. The results, as shown in Chapter 4, are indeed able to model a variety of different halftone systems.

The corrected continuous tone model invoked in this paper characterizes the tone reproduction behavior of two electrophotographic printers. The corrections that were applied were heuristic, but the result appears to correlate with physical expectation. In particular, the apparent minimum in the spatial efficiency parameter, A, corresponds qualitatively with expectation based on the MTF characteristics of paper. In addition, the values of S and of ε_o that fit the data seem to make intuitive sense. One would expect the cyan toner used in color reproduction to have a very low scattering coefficient in order to be able to color mix reliably with yellow and magenta toner to make reasonably high chroma colors. The black toner, on the other hand, does not necessarily have to have a low scattering coefficient. But a significant scattering coefficient means the absorption

coefficient, ε_0, should be higher in order to make up for the effect of scattering.

In summary, the parameters in Table 4.1 make good qualitative sense. However, the model does not show as strong a correlation with LPI as one might expect, and the difference in behavior between the cyan and the black in Figure 4.13 for A versus F_n does not make sense. One might attribute the difference to experimental error, but it is probably more reasonable to acknowledge that the model is still in a preliminary stage and is still quite heuristic. In spite of this, the model does provide a good fit to a wide range of halftone types. Thus it would appear quite justified to explore the potential utility of the modified continuous tone strategy for modeling color and tone reproduction in halftones.

Further investigation of the continuous tone model might include a closer analysis of the assumptions implicit to the model presented in this project. Two key assumptions recommended for further study are as follows.

- The Ink delivery function for coverage, C, versus F_n, is assumed to be a fixed characteristic of the printing device. It is very likely that the halftoning algorithm

chosen to print the samples may be one of the several other factors affecting this function.

- The spatial efficiency function, $f(F_n)$, is assumed to be affected only by the dot pitch, LPI. It is very likely that other factors may significantly influence the efficiency factor, and thus account for the low correlation of A versus LPI.

As a continuation of the work of this project, it is recommended that further work be done to investigate the mechanistic causes of both the toner delivery function, C vs F_n, and the toner absorption efficiency function, ε_o vs F_n. The success of the model thus far appears promising and provides a rational for further work.

Appendix A:

The experimental procedures used in this study are described in this section. The densitometry procedure to collect image reflectance, R, data is described in the first section, and the second section contains information on techniques of microdensitometry used in this project.

A.1 Densitometry

Typically, the tone behavior of a print is given as the measured reflectance versus the nominal dot area fraction, F_n, or versus the measured printed dot area fraction, F. To measure the reflectance of the printed samples, a standard densitometer was used. The densitometer was set to measure the reflective density, D. Equation (A.1) is used to convert the reflective density to reflectance, R. Table A.1, contains more information on the densitometer. The nominal dot area fraction, F_n, is already known, as it was the signal sent to the printer.

When evaluating the printing system using the cyan toner, the red-density of the samples is measured. The cyan color absorbs red

light the most and therefore, changing F_n of samples printed by cyan toner will have the most significant change in red channel of the densitometer. The density values are converted to the red-reflectance values using same equation (A.1).

$$R = 10^{-D} \tag{A.1}$$

Table A.1: Densitometer setup

Densitometer	MacBeth TR 1224
Aperture Size	2 mm
Chosen Filter	Status A
Working Mode	Reflective

A.2 Microdensitometry Analysis

The halftone modeling requires three quality metrics: Printed dot area fraction, F, Reflectance of ink or toner in the dots, R_i and Reflectance of the paper between the dots, R_p. These metrics are obtained from microdensitometry analysis. The experimental procedure involving the microdensitometry is described in this section.

The microdensitometry device used in this study consists of: a high resolution CCD video camera, microscopic optics, video capture device and a digital computer. This setup is shown in figure A.1. The CCD video camera captures and sends the image data to the digital computer. The video capture device or the frame grabber is attached to the digital computer and enables video data transfer from the camera to the computer. The captured image data can be stored as various image formats (eg. TIFF-Tagged Image File Format or BMP-bitmapped file). When analyzing the samples printed by black toner, an 8-bit grayscale bitmapped file format (.BMP) is used to save the captured images. To save the microdensitometry images of the cyan toner, 24-bit RGB color TIFF file format is utilized. When using the cyan toner, only red-channel of the captured image is utilized. The software used for interface with the camera and frame grabber, and to capture the image is *Scion Image*(Release Beta 3b, 7/23/98), developed by Scion Corporation (www.scioncorp.com).

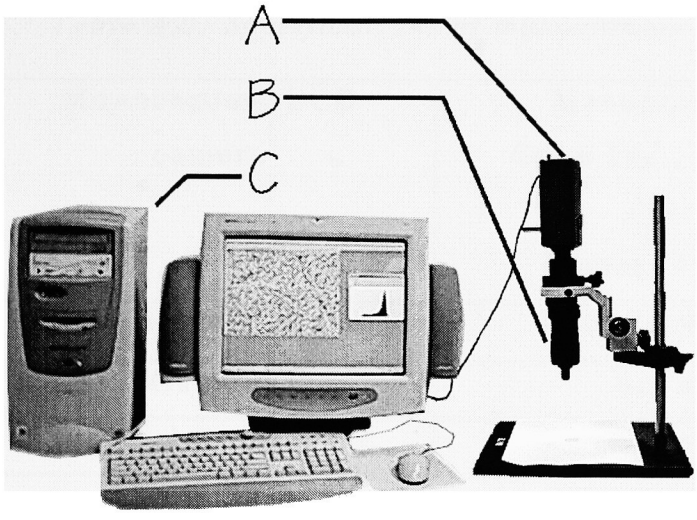

Figure A.1. Microdensitometry setup
(A) Video Camera,
(B) Optics of the camera,
(C) Computer used to receive and process images

When analyzing the prints of black toner a monochrome high resolution CCD camera is used whose specifications are given in Table A.2 and Figure A.2. To capture samples of cyan toner, a three-chip CCD color camera is used. The specification of this camera is given in Table A.3. The specification of the video frame grabber is written in Table A.4.

Table A.2: Specifications of monochrome CCD camera

Monochrome CCD camera	Manufactured by: Cohu Inc., electronics division Model: 4915-2010
Image Area	6.4 × 4.8 mm
Gamma	Set at 1.0
Spectral Sensitivity	See Figure A.2

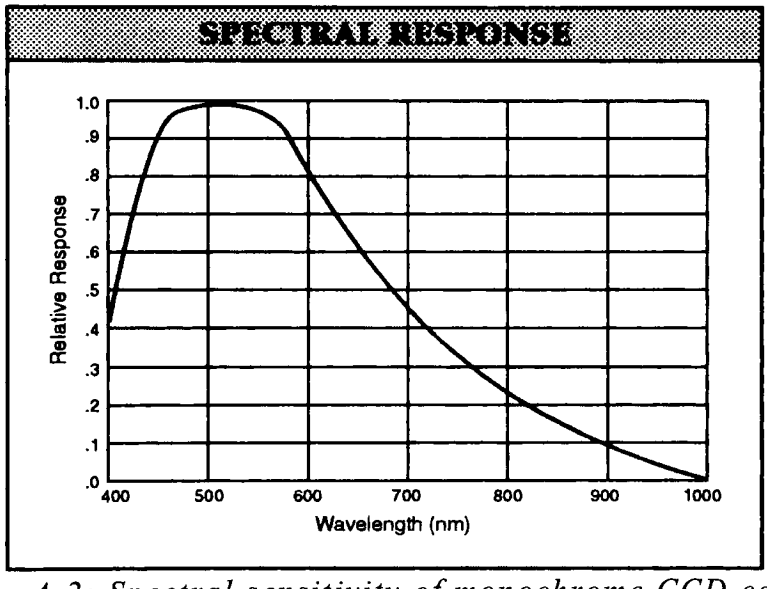

Figure A.2: Spectral sensitivity of monochrome CCD camera

Table A.3: Specifications Color CCD camera

Color CCD Camera	Manufactured by: MTI Inc. Model: DC 330
Imaging Elements	1/3", 410,000-pixel, microlens interline CCD (x3), 3 CCD, 3 Channel output, equipped with IR Filter
Gamma	1

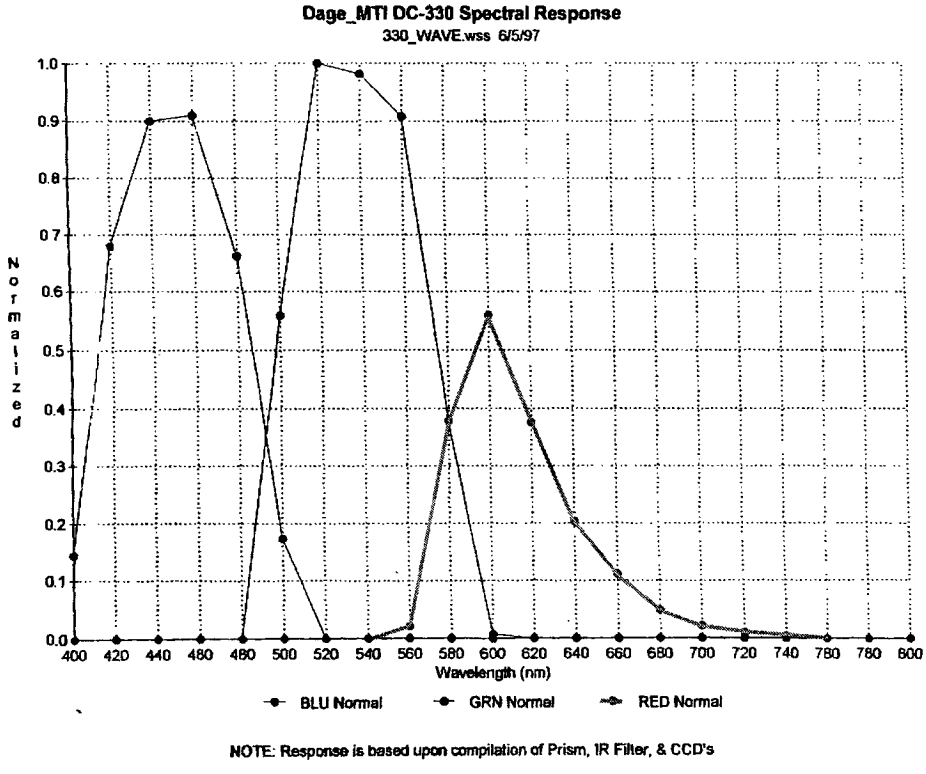

Figure A.3: Spectral sensitivity of the color CCD camera

Table A.4: Video frame grabber

Video Frame Grabber	Manufactured by: Scion Corporation Model: LG-3 for PCI bus
Resolution	640 × 480 pixels
Control software	Scion Image-Release Beta 3b, 7/23/98

When using the microdensitometry setup of the kind described above, it is required to *Flatfield* the images. It is possible that even though an object of uniform reflectance is kept in front of the camera, the captured image doesn't have the same digital value everywhere. This effect is caused by: Lens cosine effect, Non-uniform illumination, dust particles inside the optics and dark current etc. By flatfielding process, these effects can be minimized. To flatfield the captured image, a reference of known uniform reflectance and a dark image is captured. The known reflectance of the reference comes to use afterwards when calibrating the system. If captured images of the reference, dark image and the sample are Pref(x,y), Pdark(x,y) and P(x,y) respectively, the flatfielded sample

Pff(x,y) is given by equation (A.2). Note that all images have to be of the same size to perform this operation.

$$Pff(x,y) = \frac{P(x,y) - Pdark(x,y)}{Pref(x,y) - Pdark(x,y)} \cdot \frac{\sum (Pref(x,y) - Pdark(x,y))}{x \cdot y} \qquad (A.2)$$

The captured image upto this point has the pixel values in grayscale 0-255. This procedure is to calibrate the microdensitometry setup to give the images in reflectance values. If the reflectance of the reference is Rref, average pixel value of the reference image is $\overline{P}ref$ and we denote sample image converted to the reflectance values as R(x,y), this conversion can be achieved by performing operation described in equation (A.3).

$$R(x,y) = \frac{P(x,y) \cdot Rref}{\overline{P}ref} \qquad (A.3)$$

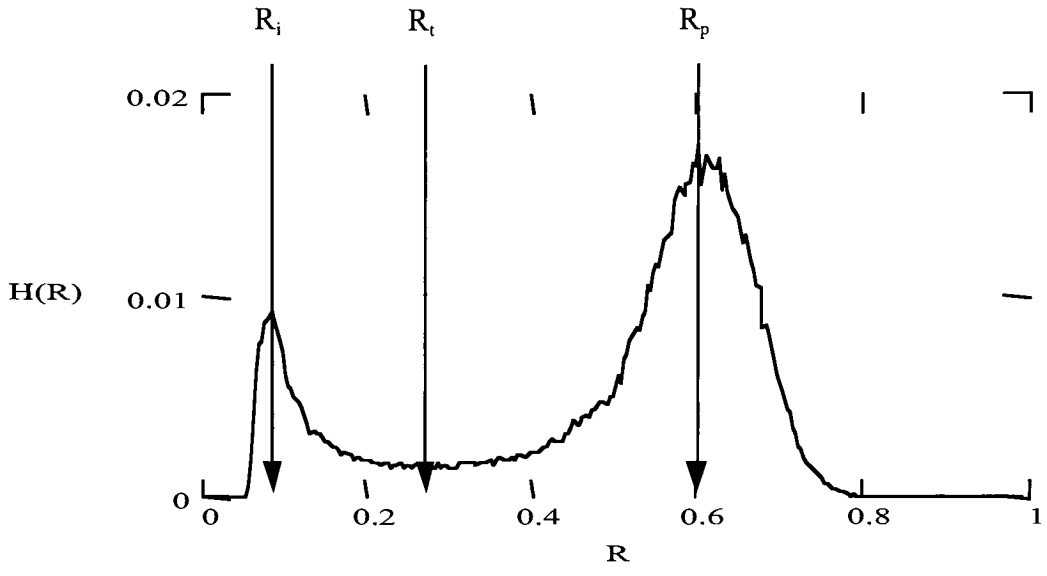

Figure A.4: Histogram of Floyd-Steinberg halftone (Fn=0.1) printed on 300dpi EP printer

To estimate the values of F, R_p and R_i, the histogram of the captured image is analyzed. As shown in figure A.4, the R_p and R_i are the local maxima. R_t is the local minimum, caused by transition from dot region to the paper region. The fraction of total pixels of reflectance values less than R_t is the measured dot area fraction, F, of the sample.

Bibliography

Arney-arney-katsube-engledrum, 1996	Arney, J S, Arney, C D, Katsube, M, Engeldrum, P: *An MTF analysis of papers*, J. Imag. Sc. Tech., vol. 40, p. 19-25, (1996).
Arney-engeldrum-zeng, 1995	Arney, J S, Engeldrum, P G, Zeng, H: *An expanded Murray-Davies Model of tone reproduction in halftone imaging*, J. of img. sc. and tech., vol. 39, p 502-508, (1995).
Arney-tsujita, 1999	Arney, J S, Tsujita, A: *Symmetry properties of halftone images I: accounting for ink opacity and dot sharpness*, J. Imaging Sc. Technol., vol. 43, p. 359 (1999).
Arney-wong, 1998	Arney, J S, Wong, Y M: *Histograms analysis of the microstructure of halftone images,* IS&T's PICS conf., p. 206-209, (1998).
Arney-wu-blehm, 1998	Arney, J S, Wu, T, Blehm, C: *Modelling the Yule-Nielsen Effect*, J. Imaging Sc., vol. 42, p. 335 (1998).
Arney-yamaguchi, 1999	Arney, J S, Yamaguchi, S: *Symmetry properties of halftone images I: scattering symmetry and pattern symmetry*, J. Imaging Sc. Technol., Vol. 43, p. 353 (1999).
Arney-yamaguchi_1, 1999	Arney, J S, Yamaguchi, S: *The physics behind the Yule-Nielsen equation,* J. Imaging Sc. Technol., IS&T-PICS conference, p. 381 (1999).
Bayer, 1973	B. E. Bayer, *An optimum method for two-level rendition of continuous-tone pictures,* Proc. of IEEE Int'l Conf. on Comm., pp. 26.11, 1973.
Berns, 2000	Berns, R: *Billmeyer and Saltzman's Principles of Color Technology*, 3rd edition, John Wiley and Sons, NY (2000).
Bruno, 1983	Bruno, M: *Pocket Pal,* 50th edition, Published by:

International Paper Co. (1983).

Clapper-yule, 1953 — Clapper, F R and Yule, J A: J. Opt. Soc. Am, vol. 43, p. 600, (1953).

Callahan, 1953 — Callahan, F P: J. Opt. Soc. Am., vol. 42, p. 104, (1952)

Dainty-shaw, 1974 — Dainty, J C and Shaw, R: *Image Science*, Academic press, NY, p. 244-258 (1974).

Engeldrum, 1996

Floyd-Steinberg, 1975 — Floyd, R W and Steinberg, L: *Adaptive algorithm for spatial grey scale*, SID Int. Sym. Digest of Tech. papers, page 36-37 (1975).

Floyd-Steinberg, 1976 — Floyd, R W and Steinberg, L: *Adaptive algorithm for spatial grey scale*, Proceedings SID, vol. 17/2, page 75-77 (1975).

Harrington, 1991 — Harrington, J S: TAGA Proceedings, 1991, p. 144

Huntsman, 1987 — Huntsman, J R: J. Imaging Technol., vol. 13, p. 136 (1987).

Kofender, 1987 — Kofender, J L: *Optical spread functions and noise characteristics of a selected paper substrates measured in typical reflection optical system configurations,* Master's thesis, Center for Imag. Sc., Rochester Inst of Tech. (1987).

Kubelka-Munk, 1931 — Kubelka, P and Mun k, F: *Ein Beitrag zur optik der Farbanstriche,* Zeitschrift für technische Phhysik, 11a, p. 593-601 (1931).

Murray, 1936 — Murray, A: *Monochrome Reproduction in Photoengraving*, Technical Report of the J. Franklin Institute, 221 (1936).

Pocketpal, 1997 — *Pocket Pal: The graphic arts production handbook,* 17th edition, Published by : International Paper

Company(1997)

Pope, 1989 — Pope, W W: TAGA Proceedings, p. 142 (1989).

Rockdeschel-hauser, 1978 — Rockdeschel, F and Hauser, O G: Appl. Opt., vol. 17, p. 3376, (1978)

Rogers, 1998 — Rogers, G L: *optical dot gain: lateral scattering probabilities,* J. Imag. Sci. Technol., vol. 42, p. 335 (1998).

Sturge-walworth-shepp, 1989 — Sturge, J, Walworth, V, Shepp, A (Editors): *Imaging Processes and Materials (Nebelette's Eighth Edition)*, Published by: Van Nostrand Reinhold, NY, US (1989).

Ulichney, 1987 — Ulichney, R: *Digital Halftoning,* Published by: The MIT press, Cambridge, MA, U.S (1987).

Viggiano, 1985 — Viggiano, J A S: TAGA Proceedings, 1985, p. 647

Wakemisha-Kunishi, 1968 — Wakemisha, H and Kunishi, T: J. Opti. Soc. Amer., *vol. 58, p. 272 (1968).*

Wilson, 1997 — Wilson, D G: *Lithography Primer*, 2nd edition, Published by: GATFPress, Pittsburgh, US (1997).

Yule-howe-altman, 1967 — Yule, J A C, Howe, D J, Altman, J H: TAPPI, Vol. 50, p 337, (1967).

Yule-Nielsen, 1951 — Yule, J A C and Nielsen, W J: The penetration of light into paper and its effect on halftone reproduction, TAGA Proceedings 3(1951):65-76